Characterising the missing thylakoid bicarbonate transport component in *Chlamydomonas reinhardtii* CO$_2$ concentrating mechanism

Chun Sing Lau

MSc by Research

University of York

Biology

Jan 2019

Abstract

Chlamydomonas reinhardtii often faces the challenge of varying CO_2 conditions in its environment. As a result, *Chlamydomonas* evolved a biophysical CO_2 concentrating mechanism (CCM) to enhance the photosynthetic performance by concentrating CO_2 around Rubisco. *Chlamydomonas* Rubisco is packaged in a unique organelle called the pyrenoid that is traversed by a network of thylakoid tubules. The current CCM model suggests that a series of membrane transporters deliver HCO_3^- across the plasma membrane, chloroplast envelope and thylakoid membranes into the thylakoid lumen. A carbonic anhydrase at the thylakoid tubule network then converts the accumulated HCO_3^- to CO_2, releasing the concentrated CO_2 at the pyrenoid. The HCO_3^- transport model therefore highlights the requirement of a HCO_3^- transporter(s) at the thylakoid membrane to allow the chloroplast stromal HCO_3^- to reach the thylakoid lumen. However, the identity of the HCO_3^- transporter at the thylakoid membrane has remained elusive. In this study, a knock-out mutant in *BST4* displayed poor growth in low CO_2 condition and exhibited reduced C_i affinity. Homology modelling showed that BST4 modelled structure resembles a Cl^-/HCO_3^- channel which belongs to the bestrophin family. The BST4 protein was localised to where the thylakoids converge at the centre of the pyrenoid. BST4 contains an extended C-terminal region with similar disorder pattern and residue profile to Rubisco-linker protein EPYC1. However pyrenoid size in *bst4* cells was similar to wild type cells, indicating that the C-terminal might not have a structural role but is most likely involved in localising BST4 to the thylakoid network at the centre of the pyrenoid. The results highlight the possibility of BST4 as the elusive HCO_3^- transporter critical to complete the CO_2 delivery route to the pyrenoid.

Table of Contents

Acknowledgements

Completing this thesis would not have been an easy task without the many help and guidance from my fellow colleagues, friends, parents and supervisor. I am extremely grateful to all of you who made this degree an incredible journey. First, I would like to thank my supervisor Dr. Luke Mackinder who has continuously pushed me to become a better scientist. Conversation with him on the CCM never failed to inspire my curiousity on this topic. Without his support, ideas and countless hours of mentoring, I would not be able to overcome the obstacles I encountered. Moreover, I would like to thank him for his brilliant Christmas gift, which is paramount to the writing of this thesis and pushes my empty coffee container collection up to a whopping 16. I would also like to thank my Co-Supervisor Dr. Gavin Thomas, who voice of experience always helps me to look at the project with clarity. Thank you giving me the opportunity to work in your lab.

I would also like to thank my fellow Lab mates, Dr. Gary Yates, Tom Emrich-Mills, Dr. Guoyan Zhao, Dr. Charlotte Walker, Dr. Irina Grouneva and many others in the Mackinder Lab and Thomas Lab for making Lab work always fun and exciting. I would like to particularly thank Dr. Gary Yates who have given so many valuable advice to my work. Discussion with him and Irina on the "Gary facts" and the human civilisation was an endless source of fun. I would also like to thank Irina for her readiness to help and experience in handling electrodes. I would like to thank Tom, for his impressive work ethic that encourages me to strive to be better. I would like to thank my bench buddy Guoyan who always bring fun news and for being a trusty source for anything PCR-related. I would also like to thank Charlotte, who always remind me the importance of a healthy diet with her commitment to an apple a day. I would like to particularly thank the staff at the technology facility, Graeme Park, Meg Stark and Karen Hodgkinson who provided microscopy training and helped with the imaging of the many cell lines. I would like to thank Dr. James Moroney for providing the fluorescent cell lines used in my work.

Many thanks to my friends Simon, Oliver and Tony who have always been there for me whenever I needed someone to talk to. I am deeply grateful to have all of you in my life. Last but not the least, I would like to thank my parents. Thank you for allowing me to pursue whatever I wanted to do in life and for encouraging me when all I needed is a little push. I would not have been able to do it without you two.

List of Figures

List of Tables

Declaration

I declare that this thesis is a presentation of original work and I am the sole author. This work has not previously been presented for an award at this, or any other, University. All sources are acknowledged as References.

Introduction

Engineering photosynthesis has great potential in improving crop yields

The growing world population has put immense pressure on food production in recent years. As more and more arable land is utilised for farming and the widespread use of fertilisers reaches saturation, the expected crop yield is unlikely to match the mounting food demand (De Bossoreille de Ribou *et al.,* 2013). Additionally, the use of fertilisers, pesticides and herbicides is expected to further contribute to soil degradation (Liebich *et al.,* 2003, Tetteh 2015) that diminish soil capacity and ultimately erode the predicted increased yield. In order to overcome these limitations, the use of genetic engineering which exploits natural variation to improve light, nutrient and water use without additional use of fertilisers and pesticides has become an increasingly popular alternative approach. In recent years, research interest has surged on the engineering of CO_2 concentrating mechanisms (CCMs) into crops, which is predicted to improve photosynthesis and yields (Covshoff and Hibberd 2012; Long *et al.,* 2015; Price *et al.,* 2013)

Rubisco is the principal carboxylation enzyme in the Calvin-Benson-Basham carbon fixation pathway. This enzyme evolved 2 billion years ago where O_2 exists as a trace gas in the atmosphere. As oxygenic photosynthesis drove the increase of O_2 concentration in the atmosphere, the efficiency of Rubisco was reduced since the increased O_2 concentration competes with CO_2 for Rubisco's active site. The oxygenation of the Rubisco substrate, Ribulose-1,5-biphosphate (RuBP) generates phosphoglycolate (2-PGA) that is recycled in a process termed photorespiration which leads to loss of nitrogen, ATP, release of fixed CO_2 and produces reactive oxygen species. This pathway results in an energy deficit to cells aside from the apparent competition of Rubisco activity (Peterhansel *et al.,* 2010). Suppression of photosynthetic efficiency due to photorespiration is even further exacerbated with rising global temperature as the catalytic preference of Rubisco for oxygenation increases and CO_2 solubility reduces simultaneously at elevated temperature.

In nature, many plants, algae and cyanobacteria have evolved ways to suppress photorespiration, most notably by operating a CCM. While the molecular machinery and structural component varies species to species, CCMs concentrate CO_2 at the active site of Rubisco, and thus suppress the oxygenation of RuBP. Recognising the potential of engineering CCM strategies to improve photosynthetic efficiencies and crop yield, projects such as RIPE (Realising increased photosynthetic efficiencies) and C4 rice project have dedicated efforts to understanding the C_4 CCM mechanism which concentrates CO_2 biochemically, namely fixing dissolved CO_2 to a 4-carbon acids (Oxaloacetate and malate).

However, the complete engineering of the biochemical CCM into crop plants is still an ongoing and complex process (Von Caemmerer *et al.,* 2012; Furbank 2016). This difficulty arises from the intricate nature of C_4 CCMs which composes of both highly regulated enzymatic components and structural differences to C3 plants. This structural component in C_4 photosynthesis termed Kranz anatomy (Sage *et al.,* 2014) is a combination of increased vascular bundle density and the elongation of the bundle sheath cells surrounding the vascular bundles. These developmental features facilitate the metabolite pool separation in C4 photosynthesis and has proven difficult to manipulate. An alternative to the biochemical CCM is a biophysical CCM which is common in diatoms, cyanobacteria and green algae. The soil and fresh-water dwelling *Chlamydomonas reinhardtii* (*Chlamydomonas* hereafter) exhibits an inducible biophysical CCM. With its quick generation time, abundance of genetic tools and chloroplast genome similarity to higher plants, *Chlamydomonas* presents not only a model organism to investigating the CCM in green algae, but also provide an attractive alternative CCM blueprint to be built in crop plants (Atkinson *et al.,* 2016; Mackinder *et al.,* 2017).

Chlamydomonas reinhardtii has an inducible biophysical CCM

Photosynthetic organisms living in an aquatic environment often experience limitations in CO_2 availability. Aside from the fact that CO_2 diffusion is 10,000 slower in water than in air, photosynthesis of neighbouring species can quickly deplete dissolved inorganic carbon (C_i) availability creating a highly variable environment. In addition, dissolved C_i exists as an equilibrium between HCO_3^-, H_2CO_3, CO_3^{2-} and CO_2 $_{(aq)}$, in a pH dependent manner (Fig. 1)

$$CO_{2(g)} + H_2O \leftrightarrow H_2CO_3 \leftrightarrow HCO_3^- + H^+ \leftrightarrow 2H^+ + CO_3^{2-}$$
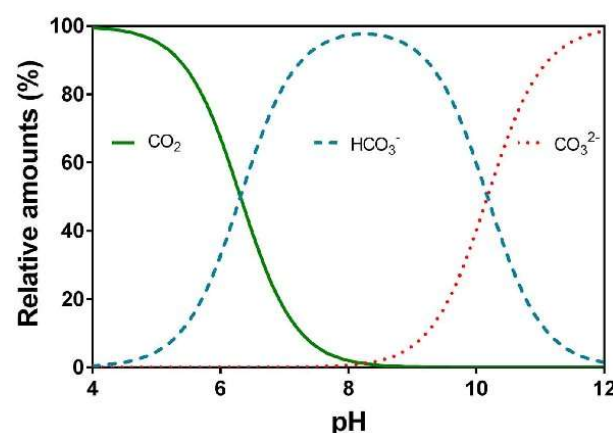
Figure 1. The relative amount of Dissolved C_i species as a function of pH condition (Figure from Pedersen *et al.,* 2013).

At the neutral pH of 7.4, the dissolved C_i species exists predominantly as HCO_3^-, which cannot cross biological membranes via passive diffusion due to its nature as a charged species (Fig. 1). This equilibrium and the slow diffusion rate of C_i restricts the photosynthetic efficiency of aquatic photosynthetic organisms as Rubisco does not use HCO_3^- as a substrate for carboxylation. To overcome this limitation, *Chlamydomonas* operates an inducible biophysical CCM which is activated by a low CO_2 condition (~0.03–0.5% CO_2; Vance and Spalding 2005). This mechanism allows *Chlamydomonas* cells to accumulate HCO_3^- at up to 40 folds greater than what is possible from passive diffusion alone (Badger *et al.,* 1980). CCM induction and operation requires coordination between structural and cellular machinery components. Briefly, the three core components of *Chlamydomonas* CCM are: (1) A HCO_3^- transport chain, which actively imports external C_i to the active site of Rubisco; (2) Carbonic anhydrases, which accelerate the slow inter-conversion of CO_2 and HCO_3^- for carbon fixation; (3) The pyrenoid, a proteinaceous subcellular microcompartment where Rubisco is concentrated.

Nucleus
Starch Granules
Chloroplast
Thylakoid
Pyrenoid
Starch sheath

High CO_2 acclimated   Low CO_2 acclimated
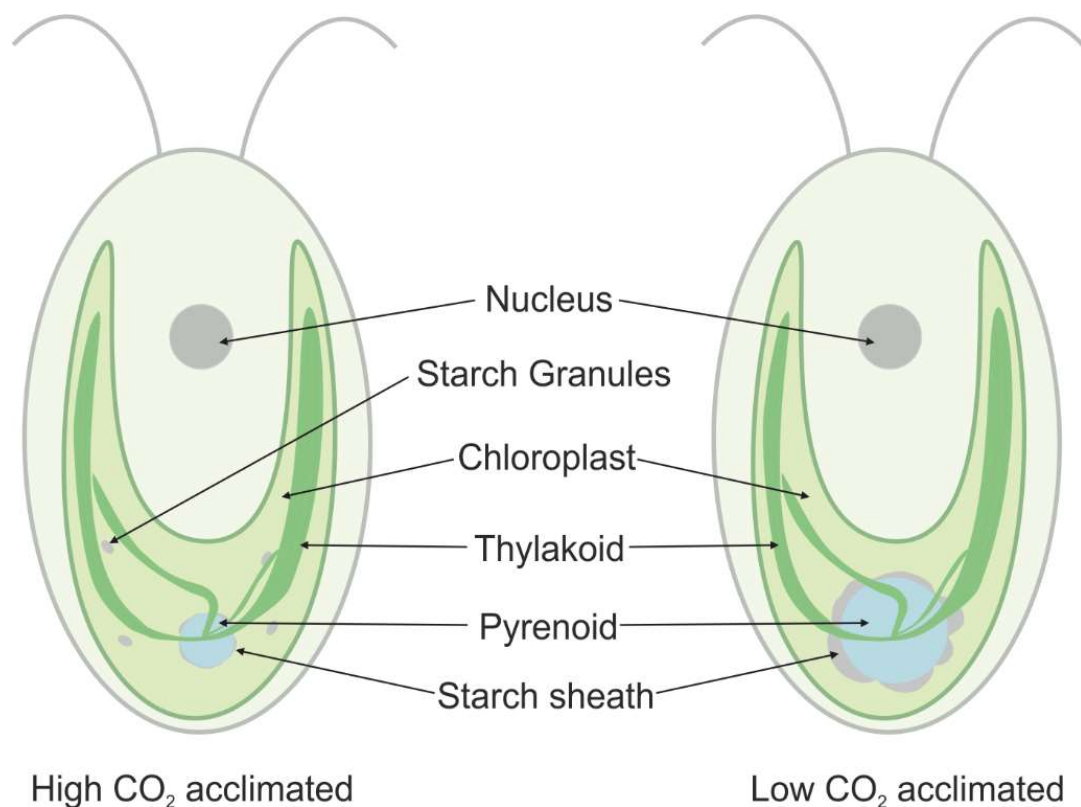
Figure 2. Structural comparison of Chlamydomonas under CCM induction. During the acclimation to Low CO_2 condition, non-pyrenoid bound Rubisco at the chloroplast stroma condensed at the pyrenoid which almost double its sizes. It is also known that the starch sheath surrounding the pyrenoid increases in thickness, and starch granule which exits between thylakoids were absent under low CO_2 condition.

Structural organisation of Chlamydomonas under CCM induction

An array of structural reorganisation occurs during the induction of the CCM. This is most obvious at the pyrenoid which is surrounded by a thick starch sheath. These two components have been found to be particularly responsive during low CO_2 acclimation (Fig. 2). While pyrenoid-less green algae species are also known to operate a functional CCM based on evidence involving C_i affinity from (Morita *et al.,* 1998), the pyrenoid in *Chlamydomonas* has been shown explicitly to be involved in the CCM (Caspari *et al.,* 2017). Pyrenoid size changes dramatically according to the surrounding CO_2 level. When grown photoautotrophically, high CO_2 grown cells contain approximately 40% of their Rubisco in the pyrenoid (Borkhsenious *et al.,* 1998), with the remaining fraction of Rubisco residing in the chloroplast stroma. However, upon exposure to limiting CO_2 condition, the pyrenoid almost doubles in area. Immunogold labelling evidence suggests that in this state the pyrenoid contains approximately 90% of all Rubisco in the cell (Borkhsenious *et al.,* 1998). While little is known on how such an increase in Rubisco content is mediated during CCM induction, this increase possibly occurs independent of translation related mechanism as there is only small changes in total Rubisco content in cells observed during the transition from high to low CO_2 (Ma *et al.,* 2011; Borkhsenious *et al.,* 1998). A recent publication has illustrated that a rubisco-linker protein called Essential Pyrenoid Component 1 (EPYC1), is crucial to Rubisco phase separation which allows pyrenoid formation (Mackinder et al, 2016). As EPYC1 is highly upregulated during acclimation to low CO_2, it is possible that this linker protein mediates the Rubisco recruitment during the low CO_2 transition in a dose-dependent mechanism.

The journey of HCO_3^- in Chlamydomonas

The journey of C_i from the external environment to Rubisco in *Chlamydomonas* is aided by an array of carbonic anhydrases and transporter components. The dominance of HCO_3^- in the neutral pH environment presents a great challenge for efficient photosynthesis under CO_2 limiting condition for algae. To combat this phenomena *Chlamydomonas* expresses a large range of carbonic anhydrases which accelerate their conversion to CO_2 and back. Moroney *et al.* (1985) discovered that whole cell affinity to inorganic carbon ($K_{0.5}$) is reduced at a high pH when cells were incubated with acetazolamide, a membrane impermeable carbonic anhydrase inhibitor, this evidence implies that periplasmic carbonic anhydrase is important to carbon uptake in *Chlamydomonas*. Using a high pH (pH 8) condition in their experiment which increased the ratio of HCO_3^-:CO_2, they postulated that this periplasmic carbonic anhydrase is dedicated to the conversion of HCO_3^- to CO_2 which subsequently

facilitates the passive diffusion of CO_2 into cells. Later, CAH1 (carbonic anhydrase 1) was identified as a periplasmic carbonic anhydrase which is upregulated by 9-fold after acclimation to low CO_2 for 3 hours (Brueggeman *et al.,* 2012) and was proposed to be the carbonic anhydrase equilibrating the external C_i (Fujiwara *et al.,* 1990; Moroney *et al.,* 1985), implicating CAH1's involvement in the CCM. However, Van and colleagues (1999) later found contradictory evidence as they observed a wild type like C_i affinity in the CAH1 knock-out strain and showed that this knock-out strain grows similar to wild type under low CO_2 condition. They suggested that despite being abundantly expressed into the periplasmic space, CAH1's carbonic anhydrase activity might not be required for C_i uptake during CCM, or is in fact compensated by other periplasmic carbonic anhydrases. Indeed, CAH2 and CAH8 have been similarly localised to the periplasm (Tachiki *et al.,* 1992; Ynalvez *et al.,* 2008). Interestingly, CAH2, which shared a >90% amino acid sequence similarity with CAH1, increased in RNA level during acclimation to high CO_2 and is absent under low CO_2 conditions (Fujiwara *et al.,* 1990). However, mRNA evidence shows a moderate amount of CAH2 transcripts are still present in low CO_2 conditions (Tachiki *et al.,* 1992). With the *in vitro* catalytic activity of CAH2 being 1.6 times greater than that of CAH1 (Tachiki *et al.,* 1992), it is possible that CAH2 compensates for CAH1 function and carries the principal role of allowing rapid interconversion of HCO_3^- and CO_2 in the external environment despite its low abundance. Similarly, a β-carbonic anhydrases CAH8 was identified with periplasmic localisation (Ynalvez *et al.,* 2008) and have also been proposed to associate with the *Chlamydomonas* CCM and can therefore carry out this proposed role in the external environment. However, as of now, no explicit evidence for periplasmic carbonic anhydrase activity has been shown to be essential for *Chlamydomonas* CCM operation and their true physiological role are yet to be fully elucidated despite obvious association with the CO_2 acclimation states. There remains the possibility of their involvement in both increasing delivery of CO_2 through locally converting abundant HCO_3^- to CO_2 and perhaps replenishing HCO_3^- that is transported into the cell.

Due to the membrane impermeability of HCO_3^-, *Chlamydomonas* expresses a system of HCO_3^- transporters/channels at each of its membranes to facilitate transport from the external environment to Rubisco in the pyrenoid. In order to probe for the genes involved in *Chlamydomonas* HCO_3^- transport, several expression profiling and transcriptomic studies have been carried out to identify genes induced by limiting CO_2 conditions (Brueggeman *et al.,* 2012; Fang *et al.,* 2012; Im and Grossman 2002; Yamano *et al.,* 2008). Nine high-light acclimated proteins have been identified in a restriction fragment differential display procedure (Im and Grossman 2002). *High-Light Activated 3* (HLA3) was identified to encode a putative ATP-binding cassette type (ABC-type) transporter belonging to the multi-drug

resistance protein family. HLA3 was also shown to increase in its mRNA transcript levels during the transition from high CO_2 to low CO_2 in addition to a light-regulated manner (Im and Grossman 2002). The up-regulation of HLA3 was later found to be regulated by CIA5, a proposed master-regulator of the CCM in C*hlamydomonas* (Fukuzawa *et al.,* 2001; Miura *et al.,* 2004) due to the inability of a *cia5* knockout mutant to grow under low CO_2 and non-responsiveness of many known CCM related genes. Using an RNAi knockdown approach, Duanmu and colleagues (2009) showed that HLA3 deficient cells exhibit impaired growth under high pH conditions where dissolved C_i exists primarily as HCO_3^- and suffers decreased C_i affinity. Additionally, *hla3* knock-out lines, made via insertional mutagenesis also showed similar phenotypes and reduced inorganic carbon affinity at alkaline pH (Yamano *et al.,* 2015). The role of HLA3 as an C_i transporter is further supported by evidence from dTALE (designed transcription activator-like effector) lines with induced HLA3 expression leading to increased C_i affinity when acclimated at high CO_2 condition (Gao *et al.,* 2015). The expression of HLA3 protein in *Xenopus* oocytes also exhibited an increase in HCO_3^- uptake capability (Atinkinson *et al.,* 2016). With fluorescent tagging and biochemical evidence establishing HLA3 localisation at the plasma membrane (Yamano *et al.,* 2015; Gao *et al.,* 2015). These results together strongly argue that HLA3 functions as a HCO_3^- transporter at the plasma membrane.

A second putative HCO_3^- transporter is also proposed at the plasma membrane. *Low inorganic carbon induced 1* (LCI1) was identified from a transcriptomic screen (Miura *et al.,* 2004). Like HLA3, its expression increases under low CO_2 conditions and is regulated by CIA5. The regulation of LCI1 by CIA5 is found to be related to a myb-transcription factor like protein, LCR1, that is proposed to function downstream of CIA5. Interestingly, LCR1 was also shown to regulate the transcript response of CAH1 (Ohnishi *et al.,* 2010). The *lcr1* mutant exhibit impaired C_i affinity at low CO_2 which can be rescued by induced expression of LCI1 (Ohnishi *et al.,* 2010). With the biochemical localisation of LCI1 at the plasma membrane (Ohnishi *et al.,* 2010), it was proposed that both HLA3 and LCI1 functions in coordinating the flow of external C_i into the cytosol. Interestingly, a recent fluorescence protein tagging and proteomics study found that these two putative C_i transporters strongly interact with each other, hinting that they may form a protein complex (Mackinder *et al.,* 2017). However, a recent conference abstract suggests that LCI1 forms a trimeric assembly and conducts flow of uncharged CO_2 species (Chou 2017), unlike the charged HCO_3^- which HLA3 is proposed to transport. While the current CCM model suggests that HCO_3^- is the main transported species across membranes during CCM induction, the existence of an active CO_2 transport system has also been suggested (Sültemeyer *et al.,* 1989). Mackinder et al., (2017) suggested that a P-type ABC transporter (Cre10.g459200) which interacts with

both HLA3 and LCI1 can coordinate H^+ flow (Thever and Saier 2009) thus creating locally alkaline regions that prevent HCO_3^- conversion to CO_2 and reduce diffusion. If such function of Cre10.g459200 is true, it will similarly generate an acidic surface to facilitate CO_2 diffusion into the cytosol via LCI1 allowing a CO_2/HCO_3^- co-uptake mechanism at the plasma-membrane (Mackinder *et al.,* 2017).

After crossing the plasma membrane, HCO_3^- must then be transported across the chloroplast membranes to reach Rubisco. The capability of active HCO_3^- transport at the chloroplast envelope has been demonstrated in isolated chloroplasts of *Chlamydomonas* (Amoroso *et al.,* 1998). Multiple HCO_3^- transporter candidates have been localized at the chloroplast envelope and have been proposed to mediate HCO_3^- transport into the chloroplast stroma. These candidates include CCP1, CCP2 were identified from a *cia5*-deficient associated transcription pool screening (Pollock *et al.,* 2004), however they were recently found to localise to the mitochondria instead (Atkinson *et al.,* 2016). The other proposed candidate LCIA, is previously recognized as a nitrogen-regulated formate-nitrate transporter *NAR1.2* and is found to be upregulated under low CO_2 conditions (Mariscal *et al.,* 2006). The two knockout mutants of LCIA, *Ain-1 and Ain-2,* were found to exhibit significant reduction in C_i affinity at an alkaline pH (pH 7.8) but not at the acidic pH (pH 6.2), implicating LCIA to HCO_3^- -related function (Yamano *et al.,* 2015). Interestingly, mRNA levels of HLA3 was also significantly reduced in the *Ain-1/2* strain and is subsequently shown to be regulated by the expression of LCIA. This retrograde regulation is likely to be mediated by a recently discovered Calcium binding protein (CAS) which re-localises from the thylakoid stroma to the pyrenoidal tubules under limiting CO_2 conditions (Wang *et al.,* 2016). As the loss of HLA3 similarly reduces C_i affinity at high pH conditions (Duanmu *et al.,* 2009a/b), the authors constructed HLA3/LCIA double insertion mutants and found that mutants exhibit further reduction in C_i affinity when compared to the LCIA single mutant. Additionally, simultaneously over-expressing HLA3 and LCIA proteins in *Chlamydomonas* increased Ci accumulation at low CO_2 conditions. LCIA's HCO_3^- transport activity was also shown when recombinantly expressed in X*enopus* oocytes (Atkinson *et al.,* 2016). These lines of evidence solidify the role of LCIA as the putative bicarbonate transporter at the chloroplast envelope.

CAH3 releases CO_2 in the pyrenoid

As Rubisco cannot utilise HCO_3^- as a substrate for carbon fixation, accumulated HCO_3^- in the chloroplast stroma must be dehydrated to CO_2 before fixation by Rubisco in the pyrenoid. However, water oxidation driven by PSII and the associated linear electron transport system generates a proton gradient across the thylakoid membrane causing the pH environment of the chloroplast stroma and thylakoid lumen to reach ~8.0 and ~5.8 respectively (Cruz *et al.,* 2005). These conditions are unfavourable for the conversion of HCO_3^- to CO_2 in the chloroplast stroma. Karlsson and colleagues (1998) found that an α-carbonic anhydrase (CAH3) located in the thylakoid fraction is crucial for growth in low CO_2 conditions. With the evidence that membrane permeant carbonic anhydrase successfully inhibit CCM function (Spalding *et al.,* 1983; William and Turpin 1987), it was proposed that the dehydration of HCO_3^- occurs in the thylakoid lumen instead of the chloroplast stroma. This role of CAH3 is further supported by the high intracellular Ci pool observed in low CO_2 acclimated *cah3* mutants despite the low CO_2 lethality (Moroney *et al.,* 1986; Duanmu *et al.,* 2009). The *cah3* mutant exhibits a phenotype that is consistent with the inability to dehydrate accumulated HCO_3^- for carbon fixation. Interestingly, an alternative function of CAH3 was also suggested. This is since a CAH3 deficient line, *cia3*, exhibit reduced *in vitro* PSII activity that is rescuable by addition of CAH3 protein (Villarejo *et al.,* 2002). It was therefore hypothesised that instead of dehydrating HCO_3^-, CAH3 facilitates hydration of CO_2 and act as a proton scavenger near the PSII assembly under high light. However, it was recently found by both Sinetova (2012) and Blanco-Rivero (2012) that CAH3 localises to the thylakoid lumen in the thylakoid minitubules that traverse the pyrenoid. Since PSII complexes are minimal in the thylakoid minitubules (Schottkowski *et al.,* 2012; Uniacke and Zerges 2007), it is unlikely that CAH3 functions solely in providing protection to PSII in high light. Hanson and colleagues (2003) further demonstrated that the *cia3* line in fact displayed excess *in vivo* PSII activity when compared to wild type, therefore provided evidence that the CAH3 principal function *in vivo* lies on providing CO_2 to the pyrenoid rather than protection to PSII during high light.

A putative CO_2 recapture system

Studies on the *bona fide* CCM components such as HLA3, LCIA, CAH3 and LCIB (Low-CO_2 induced B) have provided evidence that *Chlamydomonas* contains distinct acclimation states during limiting CO_2 conditions, with different CCM components operating under different acclimation states. LCIB-deficient mutants; *ad1* and *pmp1,* exhibit an unusual air-dier phenotype where they fail to grow in air level CO_2 (~0.04% CO_2) but survive under high and very low CO_2 conditions (<0.03% CO_2) (Wang and Spalding 2006). Their results clearly

demonstrated the distinct acclimation states of the *Chlamydomonas* CCM and showed that unique CCM components are involved at each state. Wang and Spalding (2014) also found the impact of LCIB-mutation is exacerbated at pH 6 when CO_2 is the dominant C_i species which suggests that LCIB functions in a CO_2 dependent mechanism. Combined with the observation that LCIB re-localises to the pyrenoid periphery when transitioning from high CO_2 to low CO_2 (Yamano *et al.,* 2010), This study proposed that LCIB facilitate a unidirectional hydration of CO_2 leaked from the pyrenoid at low CO_2 condition. This CO_2 recapture system is further supported by a recent report of LCIB crystal structure which found that LCIB and LCIC form a hexameric complex that resembles classic β-carbonic anhydrases (Jin *et al.,* 2016). However, the mechanistic detail of how an LCIB/LCIC mediated CO_2 uptake system can operate remains largely ambiguous, as purified LCIB/LCIC complex displays no *in vitro* carbonic anhydrase activity, and the discovery of loss of CAH3 function rescues lethal growth at low CO_2 but still display lethality at very low CO_2 (Duanmu *et al.,* 2009).

Project Aim

The aim of this study is to identify the transporter at the thylakoid membrane. As the conversion of HCO_3^- to CO_2 is unfavourable in the light-driven alkaline environment of the chloroplast stroma. The dehydration of accumulated HCO_3^- is likely to occur through the cooperative action of the thylakoid luminal localised CAH3 and acidification of the thylakoid lumen. Thus, the current models of the CCM propose that a HCO_3^- channel/transporter is present in the thylakoid membrane in order to mobilise the accumulated stromal HCO_3^- and acts to aid its subsequent release to the pyrenoid for efficient carbon fixation (Fig.3).
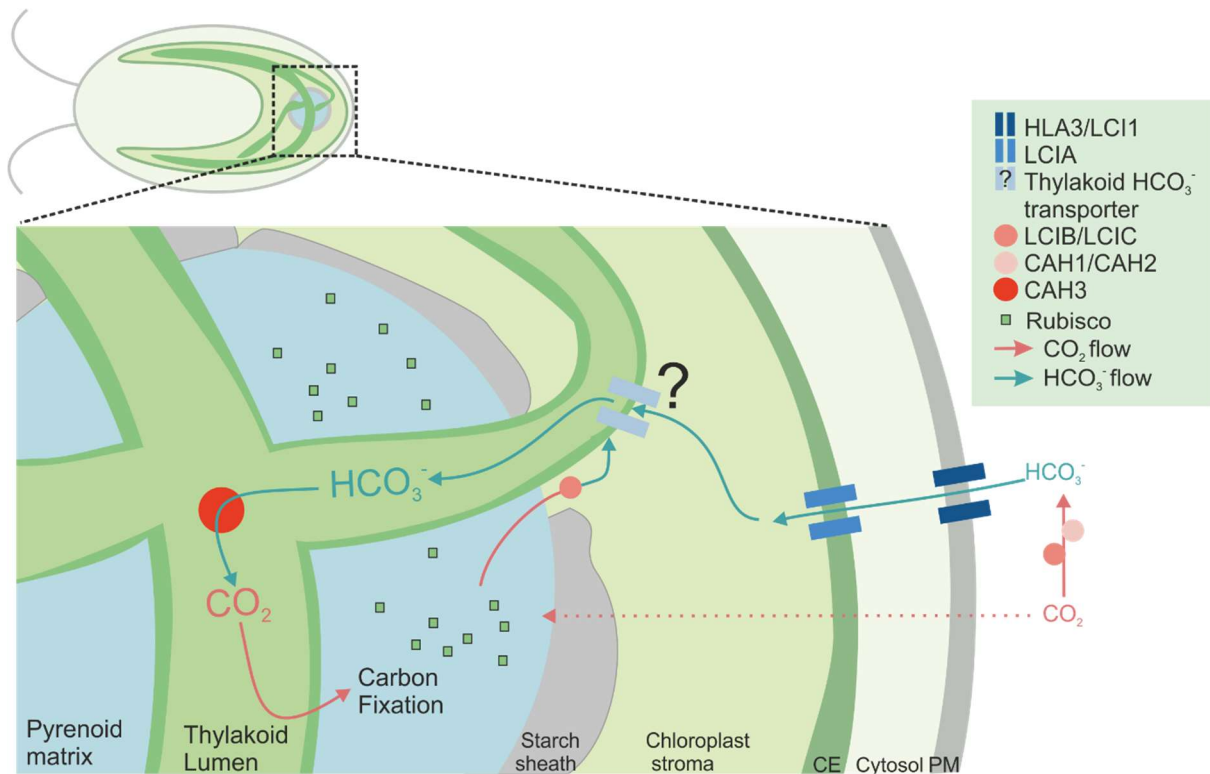
Figure 3. The current CCM model in *Chlamydomonas reinhardtii*. During CCM induction, Rubisco from chloroplast stroma concentrate to the pyrenoid at the centre of the chloroplast bowl. The HCO_3^- transporters; HLA3, LCI1, and LCIA deliver HCO_3^- to the chloroplast stroma. An unidentified HCO_3^- transporter at the thylakoid membrane shuttles HCO_3^- to the thylakoid lumen where it is released to the pyrenoid matrix after conversion to CO_2 by Carbonic anhydrase 3, (CAH3).

Previous reports have proposed that CIA8 (Inorganic carbon carrier 8) is a likely target due to the reduction in intercellular and fixed Ci in *cia8* knock-out line (Machingura *et al.,* 2017). However, the ambiguous localisation signals at the chloroplast is more reminiscent of a chloroplast stromal localisation than that of a thylakoidal membrane despite it was predicted to contain 10 transmembrane domains. However, the mutant *cia8* line exhibit a relatively weak CCM phenotype that is less comparable to other characterised mutants such as *cia3* and *lcib*. Until biochemical function of this protein is elucidated, it remains questionable whether CIA8 functions as a HCO_3^- transporter at the thylakoid membrane or other CCM-related processes. To screen for additional possible *Chlamydomonas* HCO_3^- transporters, a CCM phenotype screen was devised to identify mutants which display a low CO_2 growth defect that was rescuable by high CO_2. Identified mutants were subjected to further investigation on their photosynthetic performance and cellular architecture.

Materials and methods:

Cell culture and growth

Chlamydomonas reinhardtii wild type CW15 *mt–* (CC-4533/CMJ030) and mutant strains were obtained from the *Chlamydomonas* resource library. Tris-Acetate-Phosphate (TAP) and Tris-minimal (TP) medium pH 7.4 were prepared as described in Gorman and Levine (1965) with revised trace elements (Kropat *et al.,* 2011). 1.5% (w/v) agar was added to TAP and TP to make TAP-agar and TP-agar plates. Mutant strains were maintained on TAP-agar plates containing 20 µg mL^{-1} paromomycin. For liquid growth, starter cultures were grown by streaking strains to single colonies on TAP-agar plates. A single colony was then picked to inoculate 50 mL TAP medium in an Erlenmeyer flask under constant illumination at 50 µmol photons m^{-2} s^{-1} until reaching a cell density of 2–4×10^6 cells mL^{-1}.

Growth assay (Spot and liquid phase growth)

Starter cultures were harvested by centrifugation (600 *g*, 4 minutes, room temperature) and washed with TP medium twice. Cells were then diluted in series on 96-well plates to 10^5, 10^4 and 10^3 cells mL^{-1} with TP medium. 10 µL of diluted cultures at each concentration were spotted onto TP plates adjusted to pH 8.0, 8.2, 8.4, 8.6 and 8.8 for the pH assay or pH 7.0 and pH 8.4 for mutant growth assay. For mutant growth assay, plates were put into air-tight chambers and incubated in high (3% CO_2), low (0.04% CO_2) and very low CO_2 (0.01% CO_2) conditions at the light intensity of 50 and 150 photons m^{-2} s^{-1} for two consecutive days before increasing light intensity to 500 µmol photons m^{-2} s^{-1}. Plates for the pH assay were incubated only in low CO_2 condition. Images of plates were taken after 9 days of incubation.

For the liquid growth assay, the starter cultures were then used to inoculate a 400mL TP medium to a cell density of 2x10^5 cells mL^{-1} and were bubbled with 3% CO_2 at 150 µmols photons m^{-2} s^{-1} for 48 hours, the high CO_2 acclimated cultures were then used to inoculate separate 400mL TP medium to a cell density of 2x10^5 cells mL^{-1}. These cultures were then bubbled with 0.04% CO_2 for 6 days under continuous light of 50 and 400 µmol photons m^{-2} s^{-1}. The absorbance of cell culture was measured at 730nm with a spectrophotometer (Jenway 6300) as well as their cell density were recorded using a digital haemocytometer (Countess™ II FL) each day. To calculate doubling time, the growth rate (*k*) of the logarithmic growth phase is obtained from (Eq. 1):

$$P_{(n)} = P_{(0)}e^{kt} \qquad \text{[Equation 1]}$$

Where $P_{(0)}$ and $P_{(n)}$ is the starting and final cell density, and t is the duration of growth. The doubling time is then calculated as $(\ln 2)/k$.

Insert confirmation

Genomic DNA was extracted from a single colony grown on a TAP-agar plate. The collected colony was vortexed with 50µL of 5 mM EDTA for 30 seconds and then incubated at 100°C for 10 minutes. Primer pairs were designed to flank the predicted insertion site, obtained from the *Chlamydomonas* Library project (CLIP; https://www.chlamylibrary.org/) sequencing results. Amplification of DNA fragments were carried out as previously described by Li *et al.,* (2016). Amplified DNA fragments were purified with QIAquick PCR purification kit (Qiagen) and sent for sequencing (GATC Bioscience). Sequencing reads were analysed using Geneious software (Geneious 11.0.3)

Western blotting

Starter cultures of wild type and *bst4* were used to inoculate 400 mL of TP-medium to 1×10^5 cells mL^{-1} and bubbled with high CO_2 for 48 hours. They were then transferred to low CO_2 for 48 hours for the low CO_2 acclimated culture. The protein extraction protocol was modified from Wittkopp (Wittkopp *et al.,* 2018). Briefly, culture equivalent to 50 µg chlorophyll measured spectrophotometrically (Porra *et al.,* 1989) was harvested by centrifugation (400 rpm, 10 minutes; room temperature). The pellets were washed with wash buffer 1 (5 mM HEPES-KOH, pH 7.5; 10 mM EDTA-NaOH, pH 7.5; 1 mM Benzamadine; 1 mM PMSF; 1 mM Aminocaproic acid) and pelleted (12000 rpm, 2 minutes, room temperature). The washed pellet was re-suspended with extraction buffer 1 (5 mM HEPES-KOH, pH 7.5; 10 mM EDTA-NaOH, pH 7.5; 100 mM DTT; 100 mM Na_2CO_3) by vortex and extraction buffer 2 (5% (w/w) SDS, 30% (w/w) Sucrose) was then added. The suspensions were then boiled for 1 minute before centrifugation (12000 rpm, 10 minutes; room temperature). Supernatants of boiled sample were flashed frozen in liquid nitrogen and stored at -80 prior to use.

For western blotting, the extracted proteins were denatured at 95°C for 5 minutes in 1× Laemmeli buffer and 357.5 mM β-mercaptoethanol. The denatured proteins were separated by SDS-PAGE with a 10% polyacrylamide gel (Biorad) in running buffer (25 mM Tris-base, 192 mM Glycine , 0.1% SDS (w/v)) for 30 minutes at 60 V and then 50 minutes at 100 V. Separated proteins were electrophoretically transferred to FL-PVDF Membrane (Bio-rad) with a semi-dry blotting unit (Biorad) with transfer buffer (23 mM Tris-base, 192 mM Glycine 0.1% SDS, 20% Methanol). The membrane was blocked overnight with 5% milk in Tris-Buffered Saline supplemented with 0.1% Tween 20 (TBST). A Polyclonal antibody raised

against BST4 protein C-terminal (residues 428–443) in rabbit and monoclonal anti-α-tubulin (Sigma; T6074) raised in mouse were used to probe for their presence. The membrane was incubated with primary antibodies diluted 1:1000 with 3% milk in TBST buffer in 4 °C overnight, washed 3 times with TBST, then incubated with secondary antibodies, Alexa fluor 488 against rabbit and Alexa Fluor 555 against mouse (Thermo scientific) both diluted 1:1000 with 3% milk in TBST buffer in room temperature for 1 hour. The blotted membrane was imaged using an Amersham™ Typhoon ™ Laser Scanner 5 (GE healthcare). The excitation lasers were set at 488 and 532 with emissions from 525/50nm and 570/20 collected.

In silico *modelling of bestrophin-like proteins*

Peptide sequences of BST1-4 were obtained from Phytozome v12.1 database. Homology modelling of BST1–4 was achieved with Swiss-model webserver using *Klebsiella pneumonia* Bestrophin (PDB: 4DW8) as a template. For electrostatic potential calculation, the obtained homo-pentamer model was first submitted to energy minimization with the gromos 43B1 forcefield (Van Gunsteren *et al.,* 1996). The electrostatic potential was calculated using atom partial charge using Swiss-PDBviewer (V4.01) (Schwede *et al.,* 2003) with the solvent and protein dielectric potential set as 80 and 4 respectively. The result visualized as the electrostatic field was mapped on to the molecular surface with Swiss-PDBviewer (V4.01).

Protein Sequence analysis

Chlamydomonas Bestrophin genes were run in BLAST using NCBI genome database to probe for related genetic sequences and the bestrophin domain (Altschul *et al.,* 1990). The *Chlamydomonas, Klebsiella pneumoniae* and human bestrophin protein sequences were aligned with Geneious (V.11) using the CLUSTALW matrix. The targeting of *Chlamydomonas* was predicted by the LOCALIZER (Sperchneider *et al.,* 2017), ChloroP (Emanueisson *et al.,* 1999) and PredAlgo (Tardiff *et al.,* 2012) webservers using their full-length protein sequence. The Maximum-likelihood phylogenetic tree was generated by curating proteins with bestrophin domain annotation, the conserved bestrophin domain of each protein was isolated and aligned with Muscle-alignment software (Edgar 2004). Phylogenetic tree was constructed using the neighbour-joining method with a bootstrapping sample of 100 in the MEGAX software (Kumar *et al.,* 2018).

Inorganic carbon affinity

The photosynthetic characteristics of cell lines (total O_2 evolution and C_i affinity) were determined as previously described by Badger *et al.,* (1980). High and low CO_2 acclimated cultures were harvested by centrifugation (1000 g, 5 minutes, 4°C) and re-suspend in degassed 25 mM HEPES-KOH buffer solution (pH 7.4) to a density of 1.5×10^7 cells mL^{-1}. Cell suspension was added to a Clark-type oxygen electrode chamber (Hansatech) maintained at 25°C by a circulating water jacket. Suspensions were incubated under illumination at 400 µmol photons m^{-1} s^{-1} with constant stirring to deplete the internal carbon inorganic pool before addition of 10 µl NaHCO$_3$ at 60 second intervals. The cumulative concentrations after each NaHCO$_3$ additions were: 2.5, 5, 10, 25, 50, 100, 250, 500, 1000, and 2000 µM. The measured O_2 content in the chamber was used to calculate the rate of O_2 evolution. The measured rates were fitted using non-linear least square method to the Michaelis-Menten equation (Eq. 2) where K_m is the C_i affinity; V_{max} is the maximal O_2 evolution and [S] is the C_i concentration.

$$V_0 = \frac{V_{max}[S]}{K_m + [S]} \qquad \text{[Equation 2]}$$

Chlorophyll content of the cell suspension was determined spectrophotometrically. Briefly, 1mL of the cell suspension were harvested by centrifugation (×20320 g, 5 minutes, room temperature). Supernatants were removed and replaced by an equal amount of 100% Methanol to re-suspend the pellets before wrapping with aluminium foil. The re-suspended pellets were vortexed for 1 minute and left on ice for 10 minutes prior to harvesting as before. The chlorophyll extraction was then measured at 652 nm and 655 nm on a spectrophotometer (Jenway 6300). Total Chlorophyll content was then calculated using the empirical equation derived from Porra *et al.,* 1989.

Fluorescent-protein tagging

The BST1, 3-YFP tagged construct were provided by my supervisor Dr. Luke Mackinder, BST4-YFP tagged construct were provided by my colleague Thomas Emrich-Mills (Now at University of Sheffield) while BST2-YFP tagged construct was obtained from a collaborator, Dr. James Moroney of Louisiana State University. Transformation of wild type *Chlamydomonas* with BST1-4 fluorescent protein tagged constructs via electroporation was performed as previously described in Mackinder *et al.,* (2017). Briefly, wild type cultures were grown in TAP-liquid media under 50 µmol photons m^{-2} s^{-1} and were harvested at mid-

log phase. After discarding the supernatant cell pellets were diluted to 2×10^8 cells mL^{-1} TAP-media supplemented with 40 mM sucrose. 250 µl of the cell suspension was aliquoted into 1 mm gap electroporation cuvettes. The cell suspensions were subsequently electroporated at 800V, 20µF with a Gene Pulser II^{TM} (Biorad). Transformants were diluted to 6×10^6 cells mL^{-1} with TAP-40 mM sucrose media and incubated in the dark for 16 hours under constant shaking. The transformants were then plated on TAP-agar containing 20 µg mL^{-1} paromomycin. Paromomycin resistant colonies were re-plated into a 96 array format and screened for fluorescence using a Typhoon 8610 (GE healthcare) with the laser set at 633nm and 532nm for chlorophyll autofluorescence, and Venus fluorescence where emissions of 670/30 and 555/20 were collected correspondingly.

Confocal microscopy

Fluorescent colonies were inoculated in TAP medium to grow heterotrophically until reaching $2-4 \times 10^6$ cells mL^{-1}. The cell cultures were then harvested and re-suspended in TP medium overnight before imaging preparation. For DIC microscopy, cells were stained with Lugol's solution (KI/I$_2$) for 15 minutes before mounted on a poly-L-lysine treated glass slide. Images were captured with a LSM510 (Zeiss) with a ×63 objective (1.4 NA). Confocal Images were collected on a LSM880 (Zeiss) equipped with an Airyscan module using ×63 objective. An argon laser at 514 nm and 561 nm were used for Venus and chlorophyll excitation respectively. Emission at 525–550nm and 620–670nm were collected for Venus and chlorophyll signal, respectively. Images were deconvoluted via Airyscan processing with a filtering strength of 6 (Korobchevskaya *et al.,* 2017) in the Zeiss software. All processed images were analysed by the FIJI software.

Electron Microscopy

Starter cultures of Wild type and *bst4* were rinsed with TP medium by centrifugation (1000g, 4 minutes, 20°C). The washed cultures were then used to inoculate 400 mL TP medium to a cell density of 1×10^6 cells mL^{-1}. Diluted cultures were grown under constant illumination at 150 µmol photons m^{-2} s^{-1} and bubbled with 3% CO_2 for 48 hours to be collected as the high CO_2 acclimated cells. The cultures were then transferred to 0.04% CO_2 for another 48 hours for the low CO_2 acclimated cells. The high and low CO_2 acclimated cells were harvested by centrifugation (×1000g, 4 minutes, 20°C). Primary fixation was carried out on a rotating mixer, samples were fixed in 1.25% glutaraldehyde in 50 mM sodium cacodylate (pH 7.15) in TP medium for 15 minutes and were then transferred to 2.5% Glutaraldehyde in 50 mM cacodylate for 2 hours. Fixed samples were washed three times with 50 mM sodium cacodylate by centrifugation. Samples were then osmicated with 1% OsO_4 in 50 mM sodium

cacodylate for 1 hour on ice and washed with de-ionised water. 1% uranyl acetate in de-ionised water was used to block stain sample in the dark for 1 hour. The blocked samples were washed twice with de-ionised water and twice with 50 mM sodium cacodylate. Fixed samples were dehydrated in an acetone series (25%, 50, 75%, 90% and 100%) approximately 20 minutes each step. Dehydrated samples were infiltrated with Spurr's resin by incubating in 25% then 50% Spurr resin in acetone for 30 minutes and transferred to 75% Spurr resin in acetone for 45 minutes at room temperature. They were then incubated in 100% Spurr resin overnight before polymerising at 70 °C for 24 hours. Sections approximately 70 nm thick were collected on Copper grids and stained with saturated uranyl acetate and lead citrate. Images were collected with a FEI Tecnai 12 BT at 120kV using a Ceta camera. FIJI was used for image analysis where the area, perimeter, length of the cell, pyrenoid and thylakoids were measured. The circularity of pyrenoid is calculated by Equation 3:

$$Circularity = \frac{4\pi(Area)}{Perimeter^2} \qquad \text{[Equation 3]}$$

Results

1. Screening for High CO$_2$ requiring phenotypes

To identify new components that are required for a fully operating *Chlamydomonas* CCM, we shortlisted potential targets using a recent protein interactome study which identified novel interactors of known CCM functioning proteins such as CAH3, LCIB and HLA3 etc. (Mackinder *et al.,* 2017). In total 17 candidate genes were shortlisted and their mutants were obtained from the *Chlamydomonas* Library Project (CLiP; Li *et al.,* 2016).

Previous work on the growth of *Chlamydomonas* at high pH has shown contradicting conclusions on their viability above pH 8 (Messerli *et al.,* 2005; Hirooka *et al.,* 2017). As the the light intensity intended to be used in the mutant screening differs from these growth experiments mentioned above. A pH growth assay was carried out to determine the appropriate high pH condition for screening which also allowed robust growth of *Chlamydomonas*. Wild type was grown on TP-agar plates adjusted to pH 8.0–8.8 and then incubated under low CO$_2$ conditions. Consistent with Messerli *et al.* (2005), our wild type *Chlamydomonas* was found to be viable at all of the pH levels tested. However, an apparent reduction in growth was observed at pH condition >8.6 (Fig.4). Consequently, the pH condition of 8.4 was then chosen as the alkaline pH condition used to contrast the neutral pH 7 such that the HCO$_3^-$: CO$_2$ ratio was dramatically altered while maintaining a similar amount of growth.

To screen for a CCM-related phenotype, we incubated the obtained mutants in three CO$_2$ concentrations (Fig. 5a): 3% CO$_2$ (High CO$_2$), 0.04% (Low CO$_2$) and 0.01% (very low CO$_2$) as well as adjusted pH condition of growth medium to sift the equilibrium of dissolved C$_i$ species (as outlined above in Fig. 1).
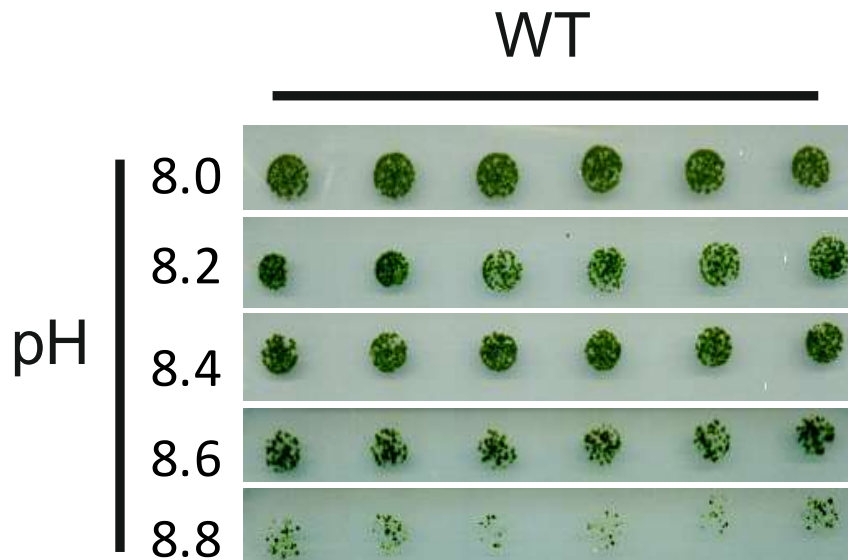
Figure 4. The pH growth assay. Starter culture of wild type were grown heterotrophically and diluted to 10^5 cells^{-1}mL$\cdot$ 10^4 cells^{-1}mL and 10^3 cells^{-1}mL before spotting on to the TP plates adjusted to pH 8.0–8.8. Colonies spotted with 10^3 cells was shown.

A large proportion of the screened mutants showed a CCM-related phenotype (Fig. 5b): of the 27 mutants screened, 14 were found to exhibit a high CO_2 requiring phenotype (Table 1: highlighted in blue), of which five mutants in this class exhibit a high CO_2 requiring phenotype independent of the pH environment during screening. cLM089 failed to grow phototrophically despite displaying no apparent growth defect in heterotrophic conditions (Supplementary Fig. 2). We found no mutants displaying phenotype exclusive to one acclimation state. Mutants which failed to grow or exhibit impaired growth under low CO_2 condition simultaneously showed similar or worse growth phenotype at very low CO_2 conditions. This includes the *LCIB* insertion mutants designated as *lcib* (cLM115), cLM114 and cLM116. The three *LCIB* insertion mutants displayed a clear growth defect at both low and very low CO_2 conditions, contrary to the expected air-dier phenotype that is observed in LCIB knockout line *ad1* (Duanmu *et al.,* 2009). This difference might be a result of incomplete disruption of the LCIB locus by the CIB1 cassette insertion, screening condition used and incorrect mapping of cassette insertion such that LCIB expression remained unaffected in the cells.
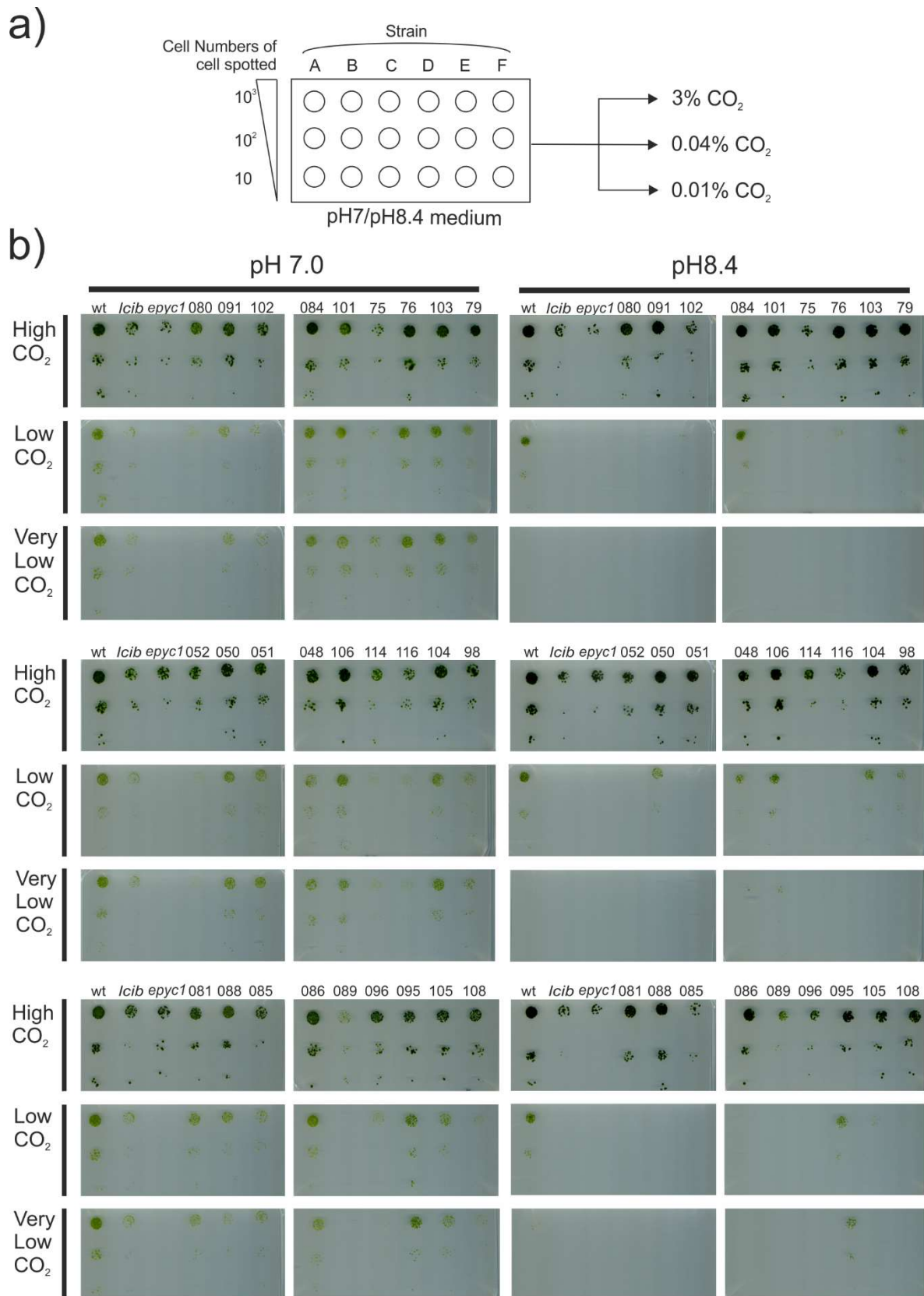
Figure 5. CCM screening of shortlisted mutants. a) The drawn schematics of the screening setup. Number of cells spotted is indicated. Plates made to pH 7.0 and 8.4 were subject to the 3 different CO_2 condition. b) Picture of screened mutants. Images of each plate were split to two halves where

the top and bottom half are shown adjacently. Strains were grown under 500 µmol photons m^{-2} s^{-1} light.

To confirm that the mutants ordered from the CLiP collection contained the CIB1 cassette in the correct genomic region, the proposed disrupted region was amplified to check for the presence of the CIB1 cassette. Primers designed to flank the predicted insert location ~200bp–500bp on both sides were used to amplify fragments using the genomic DNA (gDNA) extracted from wild type and mutant strains. PCR with wild type DNA generally yield a short 500-1000bp product in contrast to a ~3000bp product when mutant gDNA was used due to the CIB1 cassette insert. Using an elongation time of ~1 minute, amplification of fragments including the CIB1 cassette is inhibited. Comparison of amplified product size (or lack thereof) is used to determine whether mutants contain the correct CIB1 cassette insert (see below for confirmation of the CIB1 insertion site of cLM075). With the candidate genes identified with a high CO$_2$ requiring phenotype, mutants which correspond to Cre06.g261750 which encode for a protein containing a bestrophin domain were choose for further study. Since bestrophins have been previously reported to mediate HCO$_3^-$ transport activity (Qu and Hartzell 2008).

Table 1. Summary of CCM phenotype screening. The growth phenotype of strains were denoted by "++" which represent no visible difference to wild type; "+" representing slight reduction in growth relative to wild type and "–" where no growth was observed. The proposed insert location of the CIB1 cassette was obtained from the CLiP database and indicated under the location column, and the results of PCR amplification flanking the proposed region is denoted under PCR column. Rows highlighted in blue represent mutants exhibiting high-CO$_2$ requiring phenotype where CIB1 cassette insertion was also verified.

Gene	Strain number (cLM)	Strain ID	Growth					Insertion	
			pH 7			pH 8.4		Location	PCR
			HC	LC	VLC	HC	LC		
RBCS1/2 interactor									
Cre16.g655050	080	LMJ.RY0402.051387	++	-	-	++	-	Intron	Y
	091	LMJ.RY0402.121213	++	+	+	++	-	Exon	Y
Cre13.g575800	102	LMJ.RY0402.207432	++	+	+	++	-	Intron	Y
Cre06.g261750	075	LMJ.RY0402.159478	+	+	+	++	-	CDS	Y
	076	LMJ.RY0402.184445	++	++	+	++	-	3'UTR	N
	101	LMJ.RY0402.186869	++	++	+	++	+	Intron	N
	084	LMJ.RY0402.065355	++	++	++	++	++	Intron	Y
Cre08.g373450	103	LMJ.RY0402.208223	++	++	++	++	-	Intron	N
	079	LMJ.RY0402.048029	++	+	+	++	+	Intron	Y
Cre06.g249750	081	LMJ.RY0402.058741	++	+	+	++	-	Intron	N

Cre06.g271850	085	LMJ.RY0402.069506	+	+	+	++	-	Intron	Y
	088	LMJ.RY0402.085942	++	+	-	++	-	Exon	Y
Cre06.g273050	089	LMJ.RY0402.094238	+	-	-	-	-	Exon	Y
Cre12.g559250	095	LMJ.RY0402.051387	++	++	++	++	++	Intron	Y
Cre16.g663150	105	LMJ.RY0402.208438	++	+	+	++	-	Exon	Y
EPYC1 interactor									
Cre03.g202000	096	LMJ.RY0402.153726	++	-	-	+	-	Exon	Y
	106	LMJ.RY0402.0211375	++	++	++	++	++	Intron	N
HLA3 interactor									
Cre13.g571700	108	LMJ.RY0402.235547	++	-	-	++	-	5' UTR	Y
LCIB interactor									
Cre03.g206600	086	LMJ.RY0402.069780	++	++	+	++	-	3'UTR	Y
Cre01.g053950	98	LMJ.RY0402.164261	+	+	+	+	+	Intron	Y
Cre10.g452800	114	LMJ.RY0402.154803	++	-	-	-	-	Exon	N
	115	LMJ.RY0402.215132	++	-	-	-	-	5'UTR	Y
	116	LMJ.RY0402.173287	++	-	-	-	-	Exon	N
Other									
Cre10.g444700	052	/	++	-	-	++	-	Exon	Y
Cre09.g394473	050	/	++	++	++	++	+	Exon	Y
	051	/	++	++	++	++	-	Intron	Y

2. cLM075 is a BST4-deficient mutant

Bestrophin-like proteins have previously been proposed to be potential HCO_3^- transporter candidates at the thylakoid membrane in *Chlamydomonas* (Jungnick *et al.,* 2014). The CLiP mutants of this gene including cLM075, cLM076, cLM084 and cLM101 (Table 1) were obtained and subjected to the CCM screen. cLM075 grew poorly in low CO_2 conditions and this phenotype was further exacerbated at more alkaline pH (Fig 5). This increased the HCO_3^-:CO_2 ratio, which reduces the passive influx of CO_2 towards cells and therefore increase the requirement of a functioning HCO_3^- transport chain to allow efficient accumulation of C_i for growth. The growth defect observed hence likely reflects an impaired ability for HCO_3^--related processes. However, the amount of cells spotted were lower due to spotting error.

PCR amplification of the cLM101 and cLM076 proposed insertion sites (Fig. 6) gave products of the identical size with wild type, while no products were observed when amplifying the predicted site of cLM075 and cLM084 no bands (Fig. 7a) which suggests a CIB1 cassette was inserted at the amplified region of cLM75 and 84.
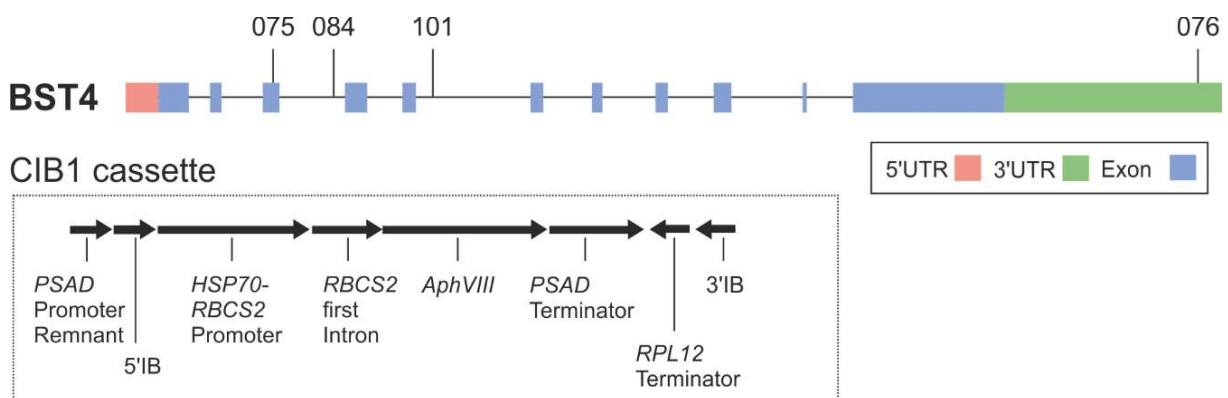
Figure 6. The proposed CIB1 cassette insert location of strains cLM075, cLM076, cLM084 and cLM101 obtained from the CLiP database.

Shown not to contain the insert at the *BST4* gene, strains cLM76 and cLM101 were not used for subsequent characterisation. To further validate the insertion location for cLM075, a ~400bp product was amplified from the 5' and 3' ends of CIB1 cassette were purified and submitted to sequencing. While the 5' amplification of CIB1 cassette was not successful (Fig. 7b). Mapping of the sequence of the purified 3' end product to the *BST4* locus showed that cLM075 contains the CIB1 cassette insert in its third exon (Fig. 7c).
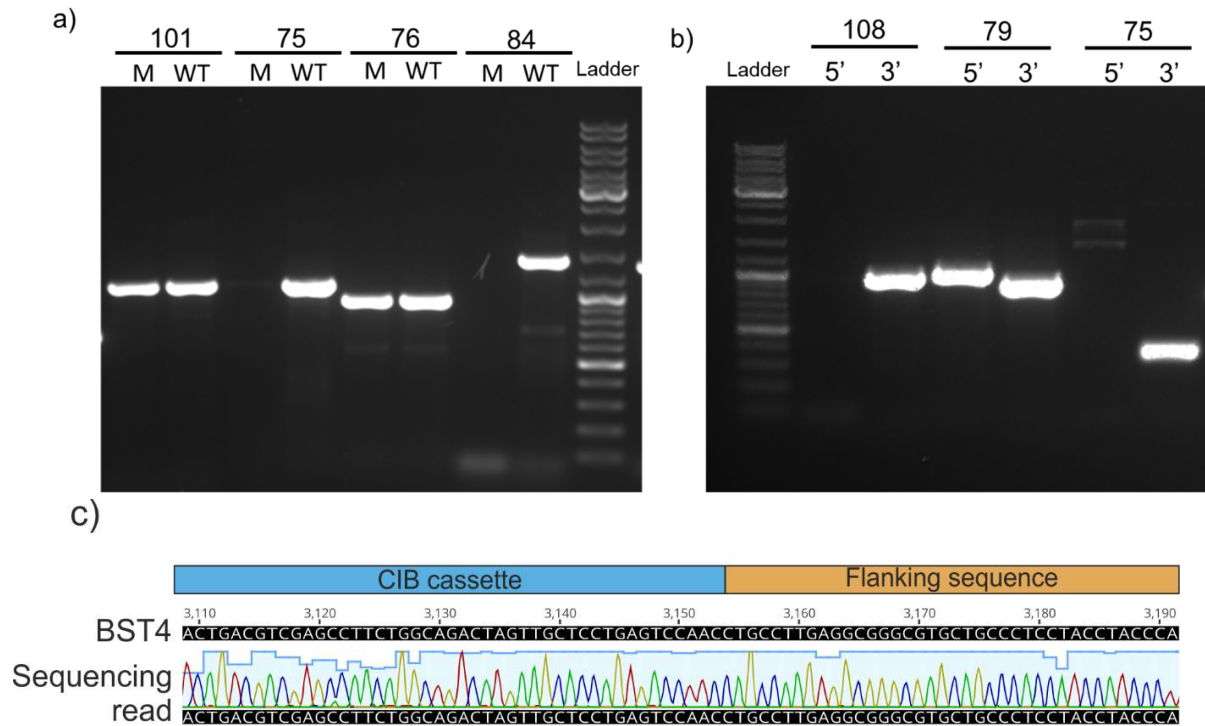
Figure 7. CIB1 cassette insert validation. a) The amplification of proposed CIB1 cassette insertion cassette site. Amplification of mutant gDNA (M) and wild type gDNA (WT) at the proposed CIB1 cassette insertion site for the corresponding mutant indicated. b) The amplification of cassette junction spanning the CIB1 cassettes and genomic DNA at both 5' and 3' sides. c) Sequencing reads of the amplified 3' cassette junction mapped on the third exon of Cre06.g261750 (*BST4*). Flanking sequence denotes the sequence predicted to flank inserted CIB1 cassette (Li *et al.,* 2014). No additional mutation was found on the sequencing read.

While insertion of the CIB1 cassette was validated, the insertion might not completely abolish transcription and may result in a reduced amount of BST4 protein present in the mutant line. To demonstrate that BST4 is absent in cLM075, the protein extracted from low CO_2 grown Wild type was separated by denaturing gel electrophoresis and immuno-blotting showed that BST4 protein migrates as a single band at ~71 kDa, matching its predicted molecular weight. This band is absent in strain cLM075 and demonstrates that BST4 is at undetectable levels in this mutant strain (Fig. 8). cLM075 was subsequently designated as *bst4*.
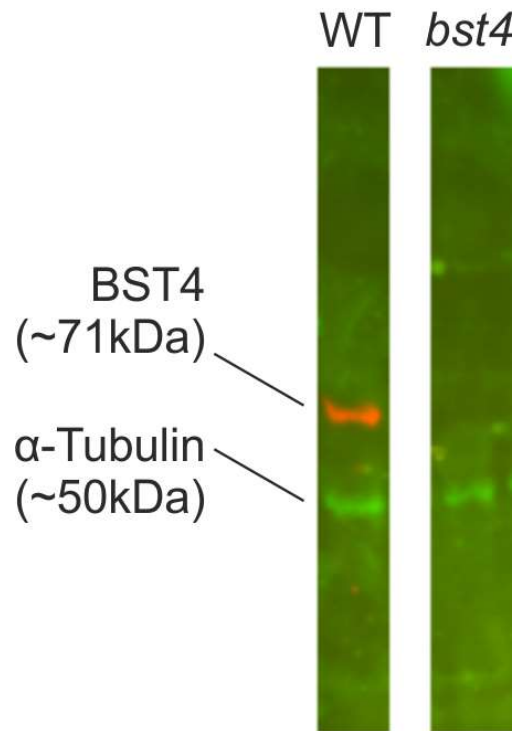
Figure 8. Western-blot analysis of total protein extracted from wild type and *bst4* strains. Wild type and *bst4* strains were grown in high CO_2 and then transferred to low CO_2 conditions for at least 36 hours prior to protein extraction. The total soluble proteins were probed with anti-BST4 antibody with alpha-tubulin as loading control. WT, Wild type.

3. The bst4 *mutant exhibits slower liquid growth in high light intensity*

To further investigate the growth characteristics of the *bst4* strains, we assayed the growth of the *bst4* mutant line under low CO_2 conditions in a liquid culture. *bst4* showed slightly reduced growth compared to wild type at ~50 μmol photons m^{-2} s^{-1} (Fig.9a) with the doubling time of wild type and *bst4* calculated to be 34.65 ± 5.98 hours and 33.96 ± 6.01 hours respectively. The light intensity used here was found to be far below the light saturation level (>500 μmol photons m^{-2} s^{-1}) previously determined (Kirst *et al.,* 2012). This led to hypothesis that differences in growth rate can be masked by a low photosynthetic rate, as little energy is generated by the low light intensity, even suboptimal efficiency for carbon assimilation will be sufficient to consume the energy generated and negate photoinhibition. The experiment was therefore subsequently repeated at a high light intensity to increase the photosynthetic rate. Indeed, when grown under the light intensity of ~400 μmol photons m^{-2} s^{-1}, the growth rate of the *bst4* strain was found to be lower than wild type (Fig 9b). The doubling time of *bst4* was calculated as 28.178 ± 3.00 hours (n=4, p=0.046, two-sample t-test), which was 1.4 times slower than that of wild type, which is 19.6825 ± 0.969 hours. It is interesting to note that

both the failure to maintain sufficient HCO_3^- transport for carbon fixation, and photoinhibition would result in the growth difference here. Regardless, the *bst4* strains showed a clear defective growth rate under low CO_2 conditions.
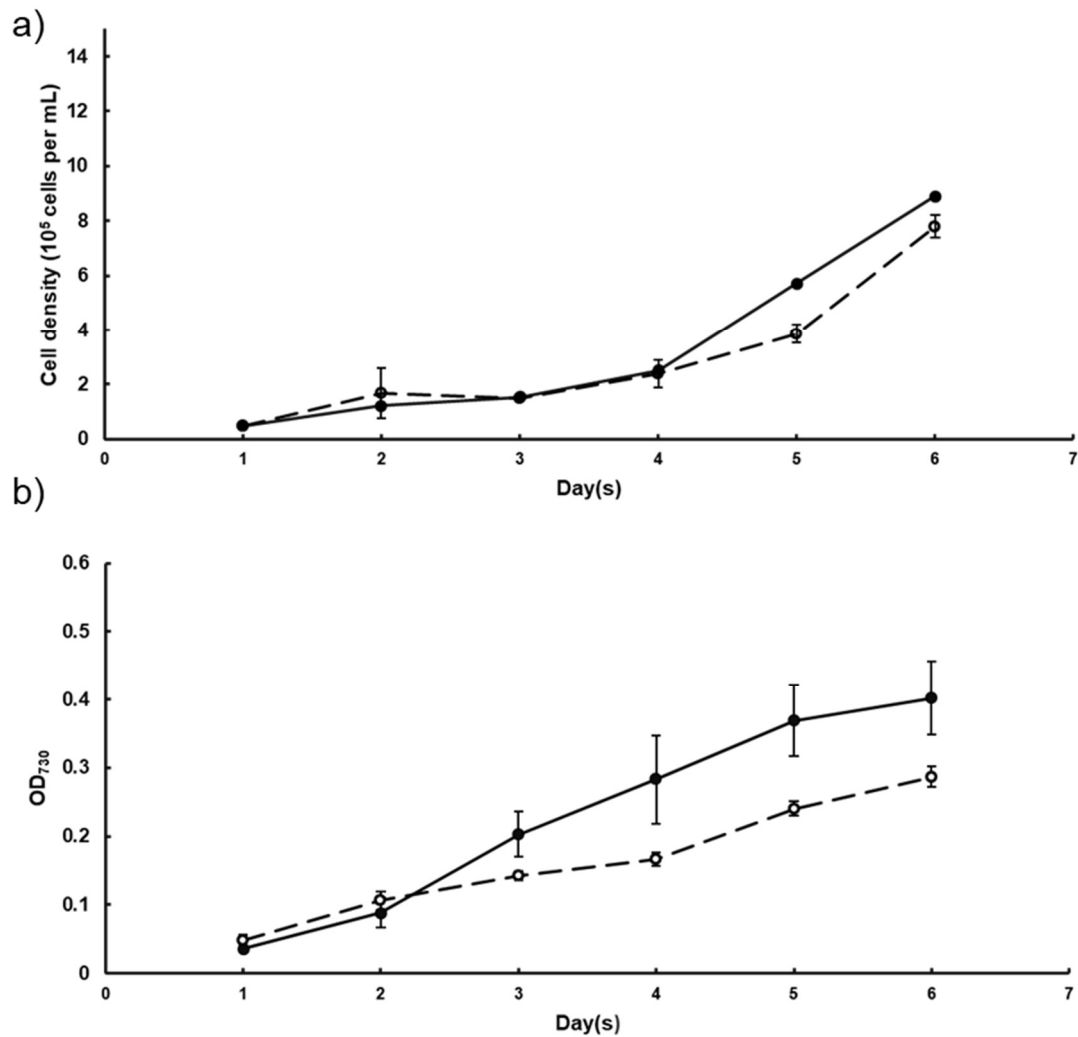
Figure 9. Liquid growth assay of *bst4* strain under low CO_2 condition. a) Growth of Wild type (closed circle, solid line) and *bst4* (open circle, dashed line) at low CO_2 under 50 μmol photons m^{-2} s^{-1} light. Data represents the mean cell density ± standard error (n=3). b) Growth of Wild type (closed circle, solid line) and *bst4* (open circle, dashed line) under 400 μmol photons m^{-2} s^{-1} light at low CO_2. Data represent the means ± standard error (n=5) of the absorbance recorded at 730 nm of using a 1 mL culture suspension.

4. Sequence analysis of Chlamydomonas *bestrophins*

The bestrophin protein lineage is widely conserved across all kingdoms (Milenkovic *et al.,* 2008; Herdean *et al.,* 2016; Fig.10). They are commonly known as chloride channels that typically contain 4 transmembrane domains. Reports on a bestrophin homolog in mouse (mBEST1) found that mBest1 displayed similar capability to transport HCO_3^- as well as Cl^- showing that bestrophins can potentially function as a HCO_3^- and Cl^- channel
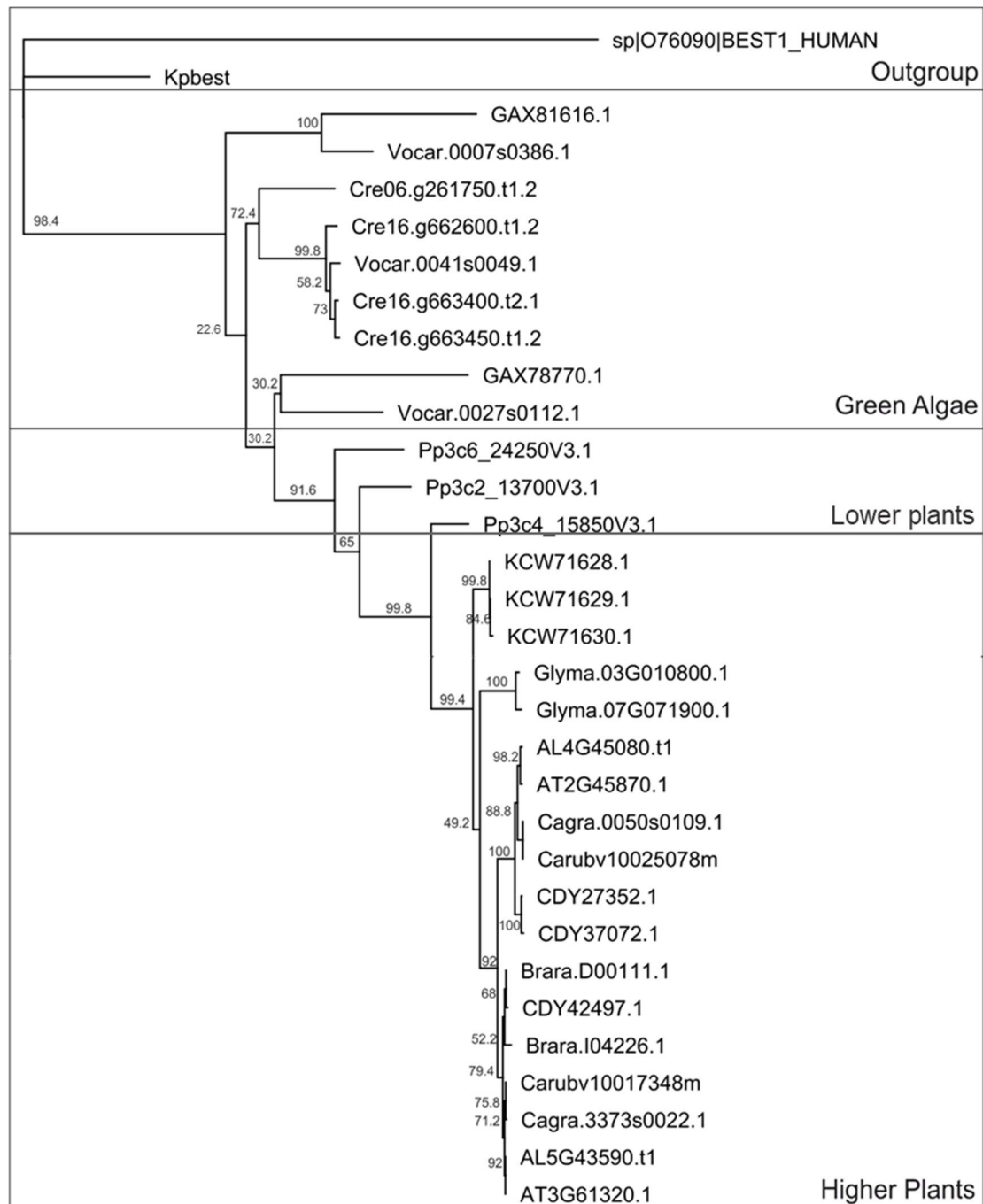
Figure 10. The molecular phylogenetic tree of Bestrophin proteins. The human bestrophin protein 1 was used as an outgroup. Phylogenies were created using neighbour-joining method with 100 bootstrapping value in MEGAX software (Kumar *et al.,* 2018). BST4 is represented by cre06.g261750. Labels at branch tip represents the Genebank/UnitProt accession number. AT: *Arabidopsis thaliana*; AL: *Arabidopsis lyrata*; Brara: *Brassica rapa*; Cagra: *Capsella grandiflora* ; Carubv: *Capsella rubella* ; CDY: ; Cre: *Chlamydomonas reinhardtii* ; Gax: *Chlamydomonas eustigma* ; Glyma: *Glycine max* ; KCW: *Eucalyptus grandis* ; Pp: Physcomitrella patens; Vocar: *Volvox carterii*.

simultaneously (Qu and Hartzell 2008). 10 genes are predicted to encode proteins annotated with a bestrophin domain in the *Chlamydomonas reinhardtii* genome (version 5.5). Three of the identified proteins, which were designated as BST1 (Cre06.g662600), BST2 (Cre06.g663400), and BST3 (Cre06.g663450) have been found to interact with LCIC/LCIB, where BST4 (Cre16.g261750) was found to interact with Rubisco (Mackinder *et al.,* 2017). To analyse the potential function of BST1–4, the characterised human (Hbest1) and *klebsiella pneumoniae* bestrophins (Kpbest) were aligned with the peptide sequences of the 4 *Chlamydomonas* proteins (Fig. 11). The annotated bestrophin domains of BST1–4 shared a high pairwise identity of 68.3% between each other. BST2 and BST3 exhibit a particularly high degree of homology, where they shared a pairwise identity of 87.9%. Additionally, BST2 and BST3 were arranged in a "head-to-tail" orientation on the genome that often corresponds to correlated expression (Li *et al.,* 2006) and is a commonly observed in gene duplication events (Reams and Roth 2015). While the bestrophin domains between BST1–4 were similar, BST4 contains an extended C-terminal tail that is ~200 residues longer than BST1–3. Previous studies on human and chicken bestrophins have suggested that bestrophin C-terminals are highly diverse and might demonstrated a regulatory role (Yang *et al.,* 2014). The long C-terminal tail in BST4 might indicate that BST4 function is distinct from BST1–3's. The alignment of BST1-4 with Kpbest and Hbest1 showed a low Pairwise identity of 38.1%. Interestingly, the human and chicken bestrophins were characterised to be activated by Ca^{2+} ions likely mediated by a calcium-clasp motif (EDDDFETNW) (Vaisey *et al.,* 2016; Dickson *et al.,* 2014). This motif (Fig. 11; highlight in red) was previously shown to be absent in the Ca^{2+} unresponsive Kpbest (Yang *et al.,* 2014). Similar to Kpbest, BST1–4 showed no sequence homology at this motif which suggests that *Chlamydomonas* bestrophins were unlikely to be regulated by Ca^{2+}.

Using the full peptide sequence of BST1–4, membrane spanning domains were searched using MEMSAT-SVM server (Nugent and Jones 2009). In total, 4 transmembrane domains were predicted in each protein. The 4 transmembrane domains were all located within the bestrophin domain (Fig. 11; high light in orange). Despite the poor sequence conservation, BST1–4 shared an identical number of transmembrane domains with Kpbest and Hbest1 and exhibit similar spacing between transmembrane domains (Fig. 11 high light in orange).

Additionally, the predicted secondary structure was also found to be largely similar to the determined crystal structure of Kpbest. (Fig. 11; Jones *et al.,* 1999).

| Secondary Structure | | | | | | |

	1	10	20	30	40	50	60
BST1	MQMQANRSSLRASPVRGLGARPLLRALPAGRVARLNVSAQAK--DPNAPIQSNPLGTLSSQSG
BST2	MQCLSSRPVAMGRAGSSALPRLP-LRAGRVCHLGVRCQAANKDPNAPIQSNPLGSFSSQLQ
BST3	MQVSKVPSSASARC----LPRLP-VRTSRVCQLSVRCQAANKDPNAPIQSNPLGSFSSQNS
BST4	MQCQLKHGAR--------------PQSQRPNWLPARAATLRPAVQHGVRRGLTLGVKAAAA
Kpbest	
Hbest1	MTITYTSQVA

| Secondary Structure | | | | | | |

	70	80	90	100	110	120
BST1	Q--VATLPRSEEARKYFRTVYDFPQWQKHRSSYRFAERLFQLSQSHILQNALPAISWWTLVAT
BST2	N--QPTLPRSEEARKYFRTVYDFPQWQTHRNQYRLMKRLFSIPQSHVIQNALPSIMWVAFTST
BST3	SGAVVTAPRNEDARKYFRTVYDFPQWQKHRSQSRLVRRLFTIPQSHVIQNALPSIMWVTFTST
BST4	PLEDKKMPADMTTRQYRRVVYDFALWAKHRDVNRYLYNLRTIIPGSRIIRQLSQPMGVVLAWAA
Kpbest	SNAMIIRPEQHWFLRLFDWHGSVLSKIIFRLLNVLMSII
Hbest1	NARLGSFSRLLLCWRGSIYKLLYGEFLIFLLCYYIIRFIYRLALTEEQQLMFEKLTLYCDSYI

| Secondary Structure | | | | | | |

	130	140	150	160	170	180
BST1	LVASYGYSYDQHMLPDVFPSISPNASCTAFISNTSVALSLLLVFRTNSSYGRWDEARKMWGGL
BST2	CVAAYMYGYDQHMLPEGFPTLAPNAACSAFISNTSVALSLLLVFRTNSSYGRWDEARKMWGGL
BST3	CVAAYMYGYDLHILPEGFPTLAPNAACSAFISNTSVALSLLLVFRTNSSYGRWDEARKMWGGL
BST4	LFGFYETCLEAGVLPSYLPKMTLMSAEPQGLT--SFALSLLLVFRTNSSYRFDEARKIWGGI
Kpbest	AIISYQWYEQLGIHLTVAP-------------FSLLGIAIAIFLGFRNSASYSRFVEARNLWGTV
Hbest1	QLIPISFVLGFYVTLVVTR-------------WWNQYENLPWPDRLMSLVSGFVEGKDEQGRL

| Secondary Structure | | | | | | |

	190	200	210	220	230	240	250
BST1	LNRSRDIMRQGATCFPDDQVEAKKALARWTVAFSRALRIHFQPEVTIESELQNILT---PAEL
BST2	LNRSRDIMRQGATCFPDDQVEAKKALARWVVAFSRALRIHFQPEVTIESELKNILT---PAEL
BST3	LNRSRDIMRQGATCFPDDQVEAKKALARWTVAFARALRIHFQPEVTIESELQNILT---PAEL
BST4	LNRARNIANQAVTFIPAEDQAGREAVGKWTVGFTRALQAHLQEDIDLRKELEKATPRWSKEEI
Kpbest	LIAERTLVRQLRNILPAEHDAHRRIVS-YLVAFSWSLKHQLRKTDPTADLRRLLPEERVTEIL
Hbest1	LRRTLIRYANLGNVLILR-SVSTAVYKRFPSAQHLVQAGFMTPAEHKQLEKLSLPHNMFWVPW

| Secondary Structure | | | | | | |

	260	270	280	290	300	310
BST1	QMLAKSQHRPVRAIHAISQIIQSVPMSSIHQQQMSNNLTFFHDVLGGCERLLRAPIPVSYTRH
BST2	QMLAKSQHRPVRAIHAISQIIQSVPMSSIHQQQMSNNLTFFHDVLGGCERLLRAPIPVSYTRH
BST3	QMLAKSQHRPVRAIHAISQIIQSVRMSSIHQQQMSNNLTFFHDVLGGCERLLRAPIPVSYTRH
BST4	DMLVNAQHRPIKAISVLSELTRQLSITQFQALQMQENCTFFYDALGGCERLLRTPIPVSYTRH
Kpbest	ASSMPTNRILLLAGNEIGQLREAGKLSDITYGLVDNKLDELAHVLGGCERLATTPVPFAYILT
Hbest1	VWFANLSMKAWLGGRIRDPILLQSLLNEMNTLRTQCGHLYAYDWISIPLVYTQVVTVAVYSFF

| Secondary Structure | | | | | | |

	320	330	340	350	360	370
BST1	TARFLFAWLTLLPFALYPTTGWGVVPVCTGIAAVLCG-IEEIGVQCEEPFG----ILPLDVIC
BST2	TARFLFAWLTLLPFALYGSCGVSVIPVCSGIAAVLCG-IEEIGVQCEEPFG----ILPLDVIC
BST3	TARFLFAWLTLLPFALYGSCGVSVIPVCSGIAAVLCG-IEEIGVQCEEPFG----ILPLDVIC
BST4	TARFLTIWLAMLPLGLWERYHWSMLPVIALIGFLLLG-IDEIGISIEEPFG----ILPLDAIC
Kpbest	LQRTVYLFCTLLPFALVGDLHYMTPFVSVFISYTFLS-WDSLAEELEDPFGTAANDLPLNAMC
Hbest1	LTCLVGRQFLNPAKAYPGHELDLVVPVFTFLQFFFYVGWLKVAEQLINPFGEDDDDDFETNWIIV

| Secondary Structure | | | | | | |

	380	390	400	410	420	430	440
BST1	NR-IIQADVMATLKDD-------------------------ADTKTILAEAGLISLIP-
BST2	NR-IIQADVMATLKDD-------------------------ADTKTILAEAGLISLRA--
BST3	NR-IIQADVMATLKDD-------------------------ADTKTVLAEAGLISLIP-
BST4	GR-AQTDVNSLLKEDPAVMKYVDDVRSGRVKSPPPLPPAPAAPAAAAAAAAARSVSPQPDV
Kpbest	NT-IIERNLLDMTGQHP-----------------------------LPE
Hbest1	DRNLQVSLLAVDEMHQD-----------------------------LPRMEPDMYWN--

| Secondary Structure | | | | | | |

	450	460	470	480	490	500
BST1	--SATS
BST2	--NSAM
BST3	--SMSL
BST4	AKTLGSLFTNVRAGVGAVAPGAPLMPQAPVRSPSPTRSVSPSFPRASAGTGMPPPVGMNGATP
Kpbest	
Hbest1	--

37

Figure 11. Amino acid sequence alignments of the bestrophin domain of *Chlamydomonas* bestrophins BST1–4 with the *Klebsiella pneumoniaea* (Kpbest) and human bestrophin 1 (Hbest1). Predicted transmembrane domains obtained via MEMSAT-SVM (Nugent and jones 2009) are highlighted in orange. Transmembrane domains of Kpbest (orange) were taken from Yang *et al.* (2015). Calcium motif (red) was obtained from Vaisey *et al.,* 2016. Secondary structure was predicted via PSIPRED V3.3. The predicted helicies of BST1–4 are represented by blue, where the solved structural helicies of Kpbest are represented by purple. Black background, identical residue in all sequences; Grey background, identical residues in >3 sequences.

To date, two bestrophin crystal structures, *Klebsiella pneumoniae* and *Gallus gallus* bestrophin, have been resolved by X-ray crystallography (Yang *et al.,* 2014; Dickson *et al.,* 2014). Using the *Klebsiella* bestrophin (Kpbest) structure as a template (Yang *et al.,* 2014), the structure of BST1–4 was modelled via the Swiss-modelling server (Fig. 12a; Waterhouse *et al.,* 2018). The calculated local QMEAN score (Qualitative Model energy Analysis; Benkert *et al.,* 2008) was used to assess (Fig. 12d) model structure quality and showed that the output structural model was of high quality. The obtained modelled structures resemble Kpbest and formed a homopentameric protein which displayed a clear central channel for ion permeation (Fig, 12b). The vase-like channel starts with the entry pocket which narrowed to a selective-pore. The selective pore then lead to a large inner cavity before narrowing again to form the aperture (Vaisey *et al.,* 2016).

Previously work on the *Drosophila* bestrophin using site-directed mutagenesis suggested that the residues that are lining the selective pore are crucial in mediating ion selectivity (Chien & Hartzell 2008). This is further illustrated in Kpbest where the ion conductance were abolished by point mutation of the pore-lining residues (Yang *et al.,* 2014). In *Chlamydomonas*, these pore-lining residues generally correspond to Leucine, Valine and Phenylalanine (Fig.12a) which are similar to those found in Kpbest (I62, I66 and F70) and in

Hbest1 (I76, F80 and F84). Interestingly, the phenylalanine at the pore lining were conserved between all the modelled *Chlamydomonas* bestrophin structures. It has been suggested that phenylalanine potentially mediates an anion-quadrupole interaction with the transporting anion which improves ion selectivity (Vaisey *et al.,* 2016; Kapoor *et al.,* 2016). The possible anion permeability of BST1–4 channels were also supported by the electrostatic potential calculation, which showed a positive electrostatic potential surface on the ion permeation channel (Fig. 12c).
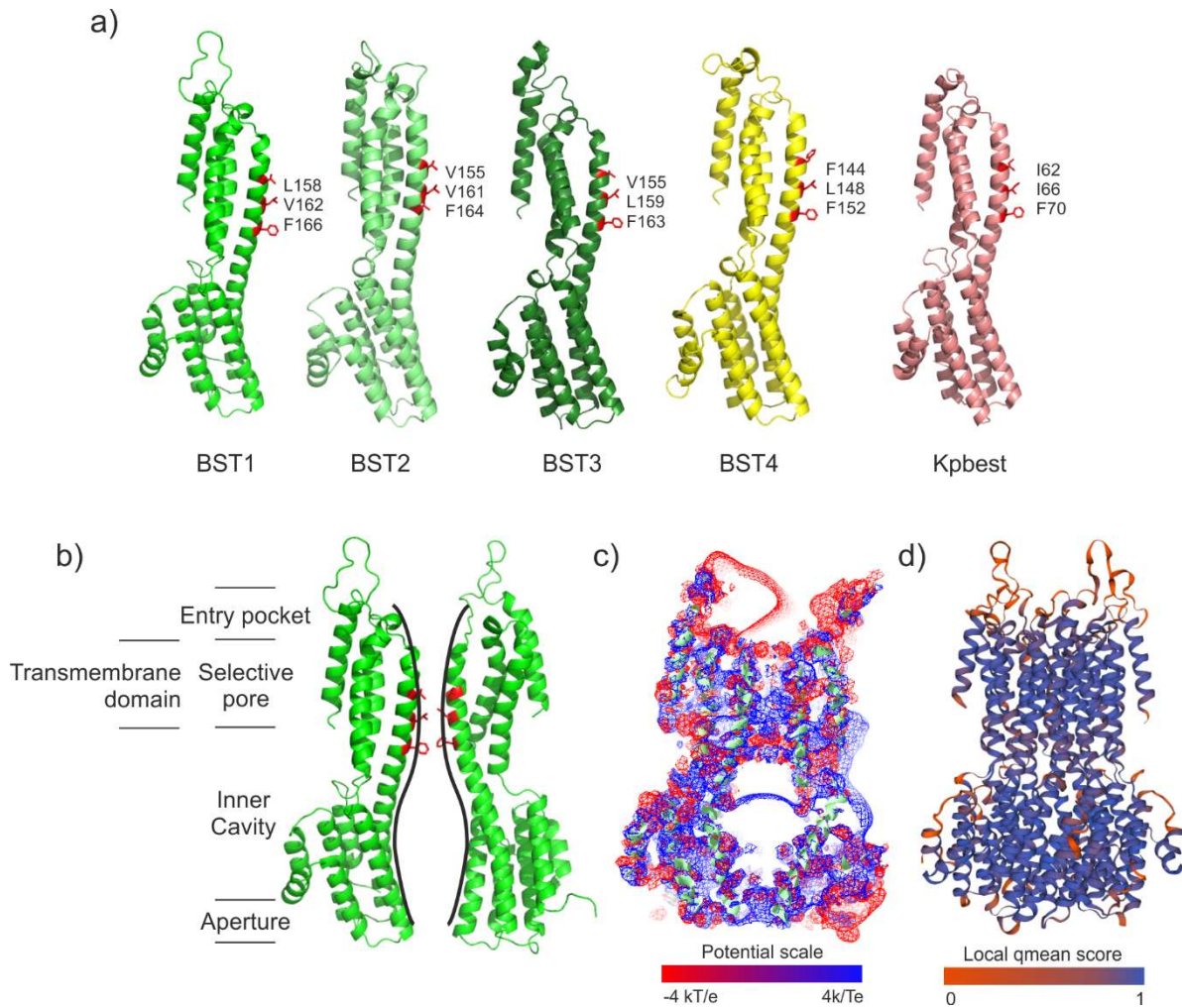
Figure 12. Modelled structure of *Chlamydomonas* bestrophins BST1-4 via Swiss-modelling server using kpbest (PDB:4WD8) as template. a) Monomer structures of BST1–4 with the critical residues highlighted as red.b) Drawn representation of the channel cavity cross-section formed from the pentameric assembly of bestrophin proteins. c) The calculated electrostatic potential of bestrophin via the Swiss-PDB viewer using partial charge with Poisson-Boltzman equation. The dielectric constant for medium and the protein was set to 80 and 4 respectively. d) BST1 pentamer structure with secondary structures coloured by the local QMEAN score, a structure quality scoring matrix.

5. BST1-4 localise to different regions of the thylakoid membrane

The full-length peptide sequences of *Chlamydomonas* bestrophins were submitted to localisation prediction webserver PredAlgo (Tardiff *et al.,* 2012), ChloroP (Emanuelsson *et al.,* 1999) and LOCALIZER (Sperchneider *et al.,* 2017). The localisation prediction of *Chlamydomonas* bestrophins largely agreed between the three prediction webservers (Table 2). All three prediction algorithms inferred that BST1, 2, 3 and 5 were localised to the chloroplast. BST4, was similarly predicted to localise to the chloroplast by PredAlgo and ChloroP, but was predicted to localise to the mitochondria by LOCALIZER. To determine the sub-cellular and organelle localisation, we fused BST1–4 with yellow fluorescent protein (YFP) and examined the fluorescent signals with confocal microscopy.

Table 2. Predicted localisation of Bestrophin proteins in *Chlamydomonas reinhardtii* bestrophins. Full length peptide sequences of Bestrophins were obtained from the Phytozhome v5.1 database. The sequences were then submitted to Predalgo, ChloroP and LOCALIZER webservers where the highest scoring prediction were listed above.

Locus	Name	Prediction Server		
		PredAlgo	ChloroP	LOCALIZER
Cre06.g662600	BST1	Chloroplast	Chloroplast	Chloroplast
Cre06.g663400	BST2	Chloroplast	Chloroplast	Chloroplast
Cre06.g663450	BST3	Chloroplast	Chloroplast	Chloroplast
Cre16.g261750	BST4	Chloroplast	Chloroplast	Mitochondria
Cre01.g038100	BST5	Chloroplast	Chloroplast	Chloroplast
Cre11.g467611	BST6	Mitochondria	Other	Other
Cre03.g199600	BST7	Other	Other	Mitochondria
Ce06.g277650	BST8	Other	Other	Nucleus
Cre07.g355300	BST9	Other	Other	Nucleus
Cre11.g474700	BST10	Other	Other	Nucleus

To localise the BST1–4 proteins, BST1-3 open reading frame was cloned to a construct containing the PSAD promoter and the C-terminal Venus tag (YFP). The BST4 open reading frame was cloned with its native promoter region and with a C-terminal Venus tag. All the constructed plasmids were transformed into wild type *Chlamydomonas* via electroporation (Fig.13a). The transformants were plated and then scanned for fluorescent colonies to be grown in TP medium (Fig.13b).
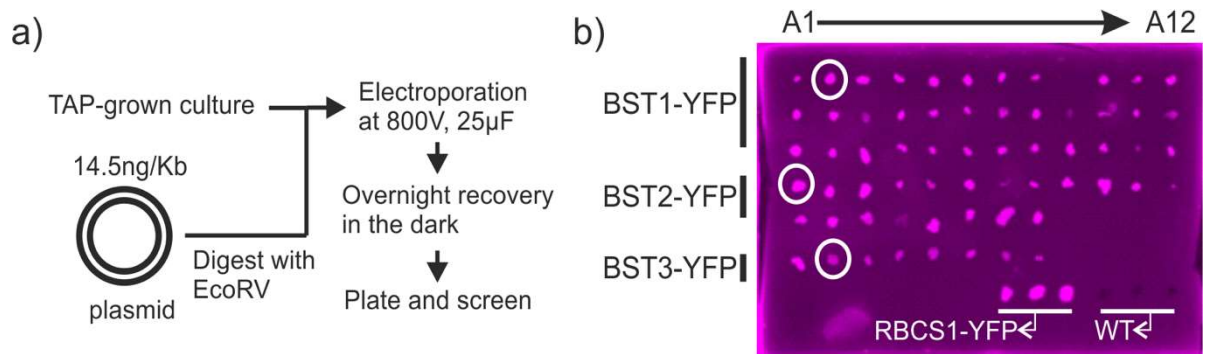
Figure 13. Transformation of fluorescent protein tagged construct into Wild type *Chlamydomonas*. (a) The transformation workflow of fluorescent tagging plasmid. (b) Fluorescent colonies pooled from the selection plate after transformation. Selection plates were screened with Typhoon 8610 with laser set at 532 and laser setting of 525/50nm. Colonies circled indicate colonies selected for confocal imaging. RBCS1 (Rubisco small subunit 1)-YFP tagged lines and Wild type were used as controls.

Confocal imaging of these fluorescent lines showed that the localisation of BST1–4 agrees with the chloroplastic localisation prediction (Table 2). Both BST1–3 and BST4 YFP-tagged lines were devoid of signals at the chloroplast membrane, however they were localised to different regions of the thylakoid membrane. For BST1-3-YFP tagged lines, I observed a non-homogenous chloroplastic signal that vastly overlap with the chlorophyll signals, which infer their location on the thylakoid membrane. The observed signals were also enriched around the pyrenoid and extend towards the pyrenoid matrix (Fig.14b; Blue arrows). Albeit to a smaller extent, the fluorescence signals of tagged BST proteins formed a tubule-like/spot structure that was reminiscent of the thylakoid tubules that traverse the pyrenoid matrix (Engel et al, 2015) much like the outer-pyrenoidal signal observed from the PSAH YFP-tagged line (Fig. 14a). These fluorescent patterns strongly suggested that BST1–3 are localised in the thylakoid membrane. Signals observed from the BST4 YFP-tagged lines were shown to concentrate at the pyrenoid. However, unlike the signals observed from Rubisco small subunit (Fig.14a; RBCS1-YFP) which occupies the whole of pyrenoid. The BST4 signals were much less extensive at the pyrenoid, restricting to only the central area. Strikingly, the BST4-signals seemed to form a star-shaped resembling the Calcium Signalling Peptide, CAS, which is localised to the thylakoid (Wang *et al.,* 2016). With its transmembrane domain, BST4 is most likely localised to the thylakoid tubules that traverse the pyrenoid matrix.
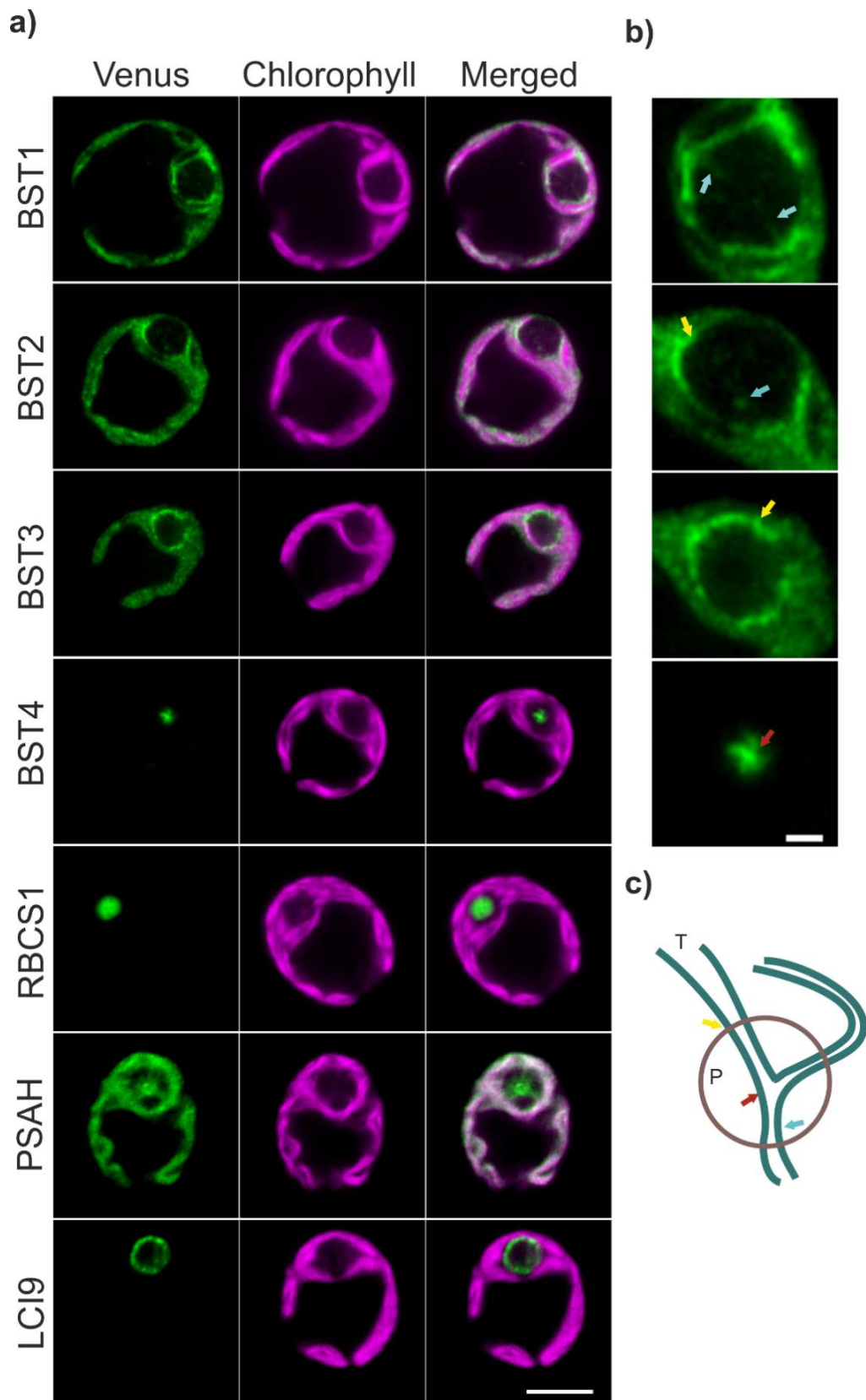
Figure 14. Localisation of the fluorescently tagged bestrophin proteins. a) BST1-4 localisation images and representative images of proteins localised to the chloroplast. Scale bar 5µm. b) Representative images of BST1–4 with the regions of pyrenoid enlarged. Scale bar: 1µm. c) The drawn

representation of the BST1-4 signals at the thylakoid knot (Red arrow), thylakoid traversing pyrenoid matrix (blue arrow) and pyrenoid periphery (yellow arrow).

The similarity between CAS and BST4-YFP signals pattern prompted us to examine whether BST4 exhibits similar re-localisation behaviour under dark where the CCM is suppressed. The BST4-YFP tagged strains were grown as described above. The strain was mounted and kept under moderate light (150 µmol photons m^{-2} s^{-1}) briefly for 10 minutes before being imaged such that cells recover from the temporary shading during sample preparation. Cells were initially imaged in the light and were then left in complete darkness for 10 minutes before the next image was captured. Four images were taken sequentially every 10 minutes. It was found that, other than the sequentially decreasing fluorescence intensity of BST4-YFP signals that was likely due to photobleaching, no re-localisation of BST4-signals was observed during a light to dark transition. (Fig.15).
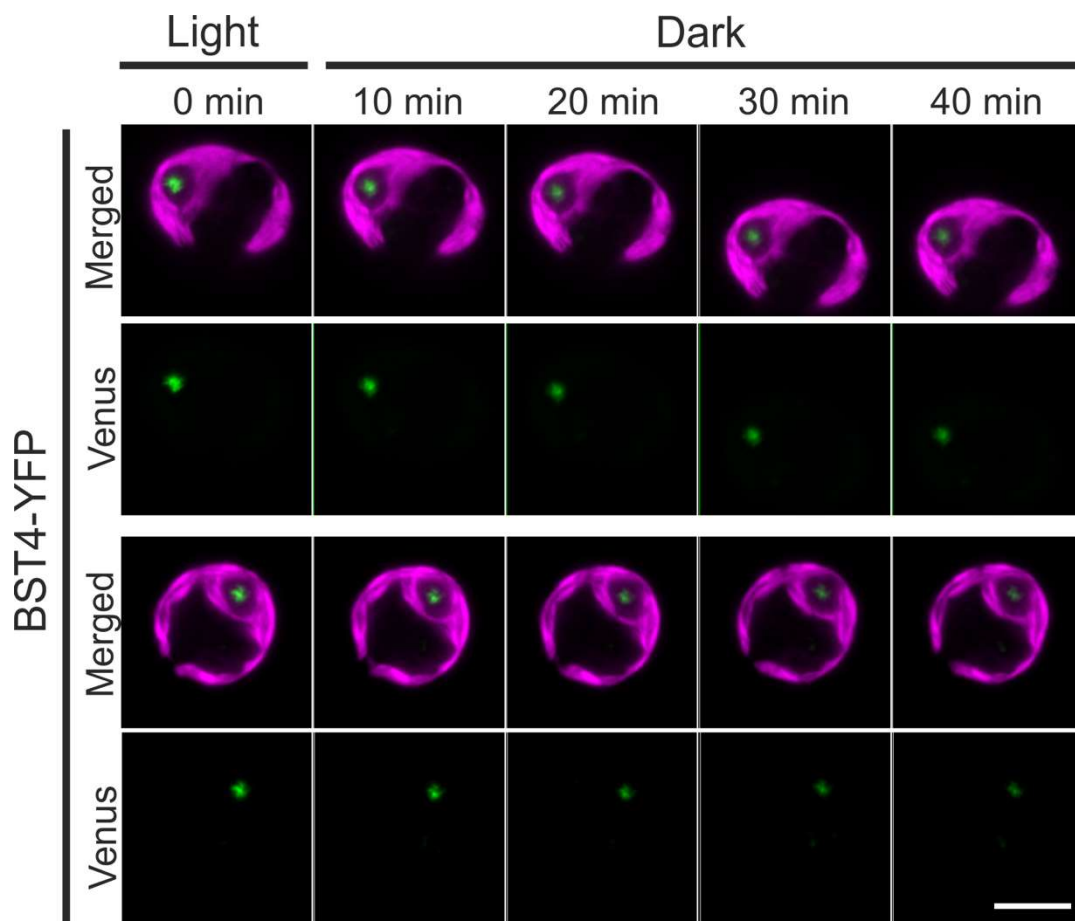

Figure 15. Localisation of BST4 during light to dark transition. BST4-YFP tagged strains were grown in low CO_2 under moderate light condition (50 µmol photons s^{-1} m^{-2}). Cells were mounted to and first imaged in the light and were then kept under dark for the remainder of imaging. Two representative cells are shown. Scale bar: 5 µm.

6. bst4 exhibits reduced Ci affinity under Low CO_2 conditions

Operation of the CCM promotes active HCO_3^- transport and accumulation of CO_2 at the site of rubisco, this is reflected by the drastically increased whole cell affinity towards C_i by approximately 10–20 fold as cells encounter C_i limiting conditions (Amoroso *et al.,* 1998). To evaluate whether the inability of *bst4* mutant to grow under low CO_2 at high pH stems from an impaired CCM, its photosynthetic characteristics was probed via C_i dependent photosynthetic O_2 evolution. Wild type and *bst4* cells were grown phototrophically in high CO_2 until the cell density reached early mid-log phase prior to their O_2 evolution measurement, cultures were then acclimated to low CO_2 by bubbling with 0.04% CO_2 for a further 36 hours before additional measurements.

Table 3. The photosynthetic characteristics of Wild type and *bst4*. Maximal O_2 evolution activity (V_{max}) and C_i affinity $K_{0.5}$ of Wild type and *bst4* cells were calculated by a least square fitting method with the Michaelis-Menten equation. Results were calculated from two independent experiments for a total of six technical replicates. Data below represented the mean value ± standard error.

CO₂ acclimation condition	V_{max} (µmol O2 mg Chl^{-1} hr^{-1})		$K_{0.5}$ [Ci] (µM)	
	Wild type	*bst4*	**Wild type**	*bst4*
High CO_2	31.65 ± 1.35	29.19 ± 2.04	206.87 ± 9.14	254.53 ± 35.31
Low CO_2	18.17 ± 0.84	18.17 ± 0.90	20.23 ± 3.78	58.67 ± 9.26

The $K_{0.5}$ value, corresponding to the C_i concentration required to reach half maximal O_2 evolution rate were found to be similar between the High CO_2 acclimated cells of Wild type and *bst4* strains (Table 3). This is different under low CO_2 condition, where the $K_{0.5}$ value for *bst4* strains, 58.68 ± 9.26 (Mean ± SE), was almost three times higher than that of the wild type, which has a $K_{0.5}$ of 20.23 ± 3.78. This shows that the *bst4* strains displays a lower affinity to C_i compared to wild type once the CCM is induced (p=0.0049, n=6, *two-sample t-test*) and suggests that the *bst4* mutant has a defective CCM.
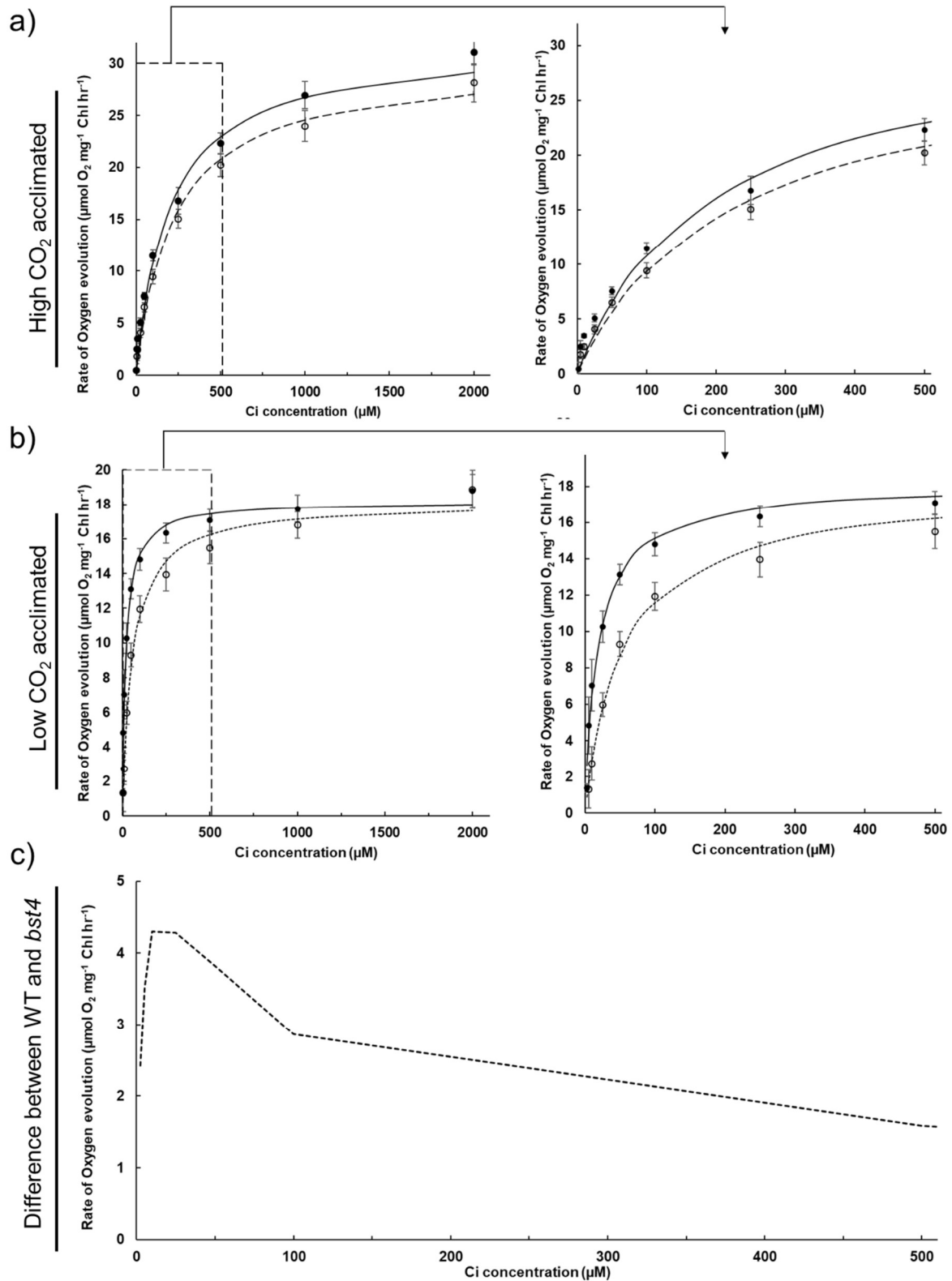
Figure 16. C_i dependent photosynthetic O_2 evolution assay at pH 7.4. (a) High CO_2 acclimated and (b) Low CO_2 acclimated cultures were assayed across a range of C_i concentrations, with wild type represented as closed circles and *bst4* represented by open circles. To facilitate analysis, the squared region denoting the lower C_i concentration region was re-plotted adjacently. Data points represent the mean calculated O_2 evolution rate and their standard error, where the plotted lines represent the

modelled Michaelis-Menten curve. (c) Difference in mean O_2 evolution rate between wild type and *bst4* across the lower C_i range.

A closer look at the O_2 evolution rates between the two strains showed that the *bst4* strains were particularly inhibited at the C_i concentration in the range of 25 µM – 100 µM, as shown by the large difference between wild type and *bst4* activity (Fig. 16c). The C_i concentration range indicated above is equivalent to the low CO_2 condition. This inhibition at the 25 µM – 100 µM [C_i] range was minimal in high CO_2 acclimated cells (Fig 16a) and was alleviated in low CO_2 acclimated cells when the C_i concentration increased to 200 µM and returned to a wild type rates at a C_i concentration range >500 µM, where a saturating amount of Ci is present (Fig 16d). Additionally, the inhibition of O_2 evolution rate was found to be less prominent when C_i concentration <25 µM, which suggests that the loss of BST4 has caused a defect most pronounced at the low CO_2 condition.

The maximal O_2 evolution activity (V_{max}) did not differ between strains in high CO_2 acclimated (*p=0.3381, n=6, two-sample t-test*) and low CO_2 (*p=0.977, n=6, two-sample t-test*) acclimated conditions (Table 3). This showed that once a saturating amount of C_i was present, where carbon assimilation was not limited by C_i transport, the photosynthetic capability between the two strains were similar. This also suggests that the photosynthetic mechanism and the associated apparatus of both strains were unimpaired and argues that the observed deficiency at low CO_2 condition in *bst4* strains is likely due to a CCM-related defects.

Next, the total chlorophyll content and the chlorophyll a/b ratio were measured, as defect in the photosynthetic apparatus could similarly result in growth defect observed. Chlorophyll content and the chlorophyll a/b ratio were determined by spectrophotometry with empirical equation derived from Porra *et al.,* 1989. Our calculations showed that on a per cell basis, the chlorophyll content between both strains were similar (Fig. 17b; p=0.7420, n=6, *two-sample t-test*). The chlorophyll a/b ratio of both wild type and *bst4* strains decreased after transition to low CO_2 conditions and their values aligned with those previously reported (2.7-2.9) at low CO_2 and (3.0-3.5) at high CO_2 acclimated conditions (Fig.17a; Polukhina *et al.,* 2016). As chlorophyll a/b ratio often reflects the state of light harvesting complexes where high a/b ratio is thought to indicate a smaller photosystem antenna size (Polukhina *et al.,* 2016), the lack of difference in pigment composition between wild type and *bst4* showed that the photosynthetic components are not altered in *bst4*. However, to truly gauge whether difference in light reaction exists between the two strains, a more detailed investigation to measure the chlorophyll fluorescence as well as PSII/PSI ratio will be required.
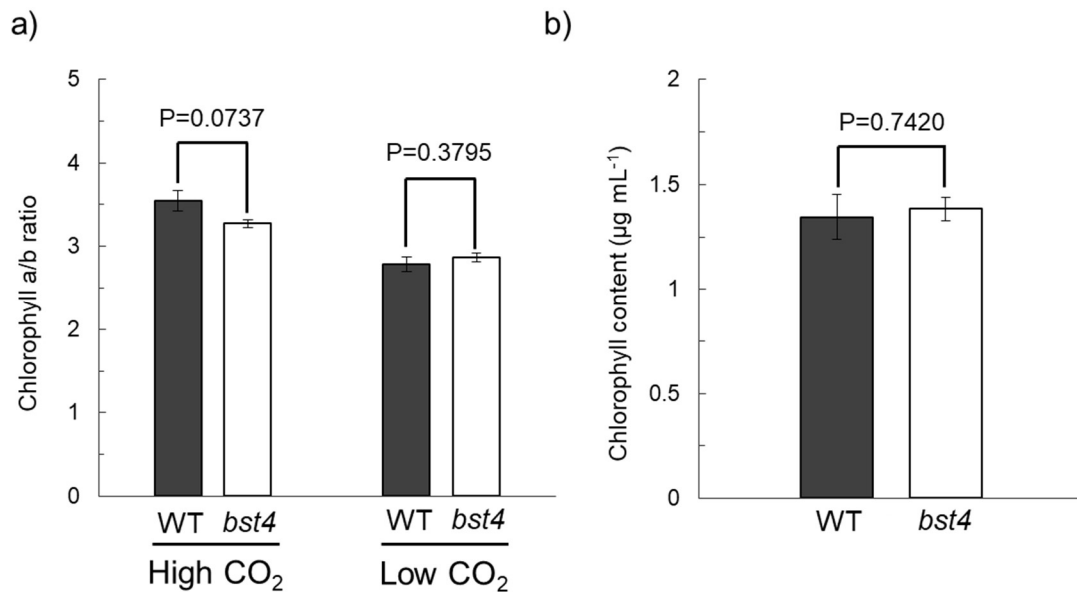
Figure 17. Pigment analysis of wild type and *bst4* strains. a) Chlorophyll a/b ratio of wild type (grey) and *bst4* (white) strains at high and low CO_2 acclimated condition. High and low CO_2 acclimated cells were grown as previously described. b) Chlorophyll content of low CO_2–grown cells taken from the liquid growth assay. Chlorophyll extraction was performed by re-suspending harvested cell pellets with 100% methanol. Chlorophyll content was measured with a spectrophotometer. The cell density was measured with haemocytometer.

7. The bst4 mutant shows no change in pyrenoid size

The C-terminal of bestrophin proteins showed very little conservation in amino acid sequence. Bestrophin C-terminals have been proposed to function in regulatory roles such as the calcium responsive loops in Hbest1 and have even been hypothesised to mediate protein-protein interactions (Tsunenari *et al.,* 2003, Xiao *et al.,* 2008). Using a sequence repeat prediction webserver called RADAR (Heger and Holm 2000), four repeats were recognised with high confidence (Fig. 18a) at the extended C-terminal of the BST4 protein that were not conserved in BST1-3 (Fig. 11). The identified repeats were predicted to be structurally disordered through DisEMBL (Linding *et al.,* 2003) programme with the remark 465 algorithm which utilise missing coordinates in the protein data bank files that likely infer disordered structure (Fig 18b). These identified disorder repeats in BST4 is similar to the rubisco linker protein, EPYC1 which consists of four almost identical repeats that are predicted to be disordered. The repeats identified from EPYC1 and BST4 protein were aligned and showed low sequence conservation between each other. Additionally, the BST4 repeats exhibited low sequence conservation to each other (Fig. 18a). Despite the low conservation found, the BST4's repeats exhibit low residue complexity where 63.1% of the residues are Alanine (26.7%), Proline (22.0%) and Serine (14.9%). This residue profile was highly reminiscent to that of EPYC1 where Serine (29.7%), Alanine (20.7%) and Proline

(10.6%) similarly take up 61.2% of the entire sequence (Fig 18c). The similarity between BST4 C-terminus and EPYC1 in their structural prediction and residue profile might suggest that they exhibit similar physiochemical properties such as the ability to mediate the liquid-like properties of the pyrenoid.
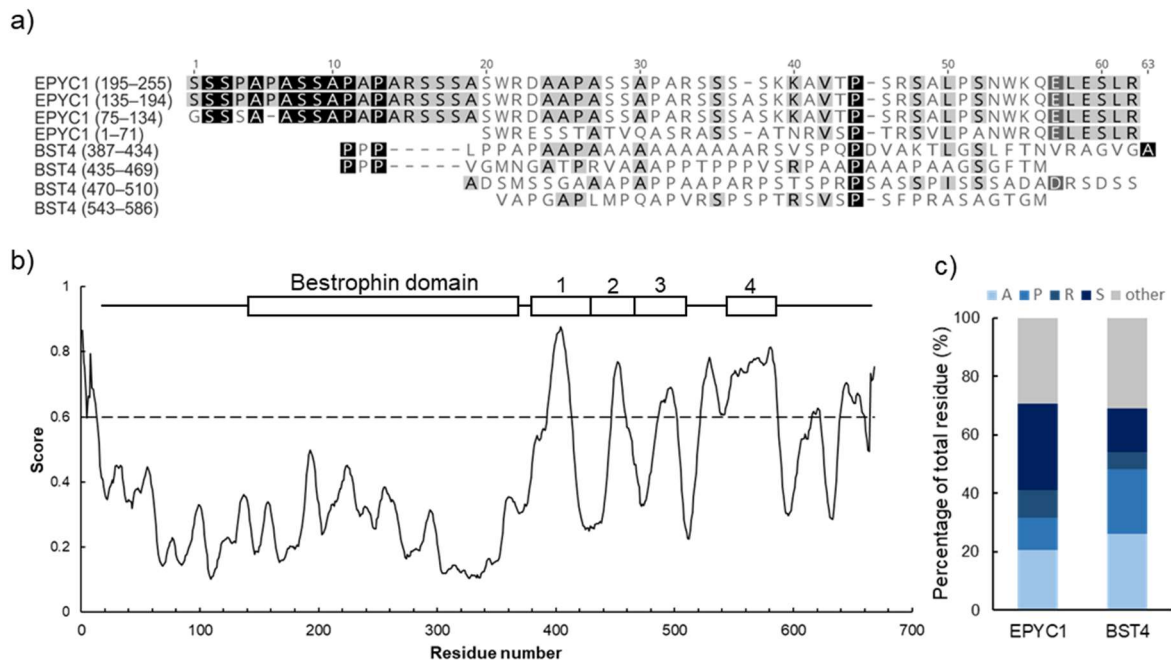

Figure 18. Sequence analysis of the C-terminal of BST4. a) Alignment of the predicted repeats of BST4 C-terminal with the four repeats from rubisco linker protein, EPYC1. 4–5 conserved residues are shown with a grey background, and identical residues across all sequence are indicated with a black background. b) Prediction of structural disorder by the 465 remark algorithm from DisEMBL-server. The benchmark score of 0.6 (broken line) was used where residues with scoring higher than that of the benchmark is considered positive. The BST4 protein sequence represented as a cartoon in proportion to the residue number was overlaid on the plot. This blocks noted as 1, 2, 3 and 4 indicate the 4 predicted repeats identified from the C-terminal domain of BST4. C) The residue profile of BST4 and EPYC1, Alanine, Proline, Arginine, Serine and other residue were coloured as sky blue, cerulean, green-blue, navy blue and grey respectively.

To investigate whether the loss of BST4 leads to altered pyrenoid structure, wild type and *bst4* strains were examined by bright-field microscopy to explore CCM associated structural changes. Wild type and *bst4* cells were grown in photoautotrophic conditions and were stained with Lugol's solution to darken the starch sheath prior to imaging. The *bst4* strains showed a clear boundary between the pyrenoid and the starch sheath (Fig 19), which was expected of the cells with a successful CCM induction as seen in wild type cells. In contrast, the *epyc1* strain which is known to fail in pyrenoid assembly exhibited no discernible boundaries between the pyrenoid and starch sheath (Fig. 19), suggesting a disrupted pyrenoid as previously described (Mackinder et al, 2016). From the bright-field images

alone, no significant differences in the CCM-related pyrenoid structure can be found between the wild type and *bst4* strain. However, subtle distinctions such as thylakoid stacking and pyrenoid size cannot be sufficiently quantify using bright-field microscopy. To examine these parameters, I grew both strains under high CO_2 and low CO_2 conditions as previously described and prepared them for transmission electron microscopy (TEM).
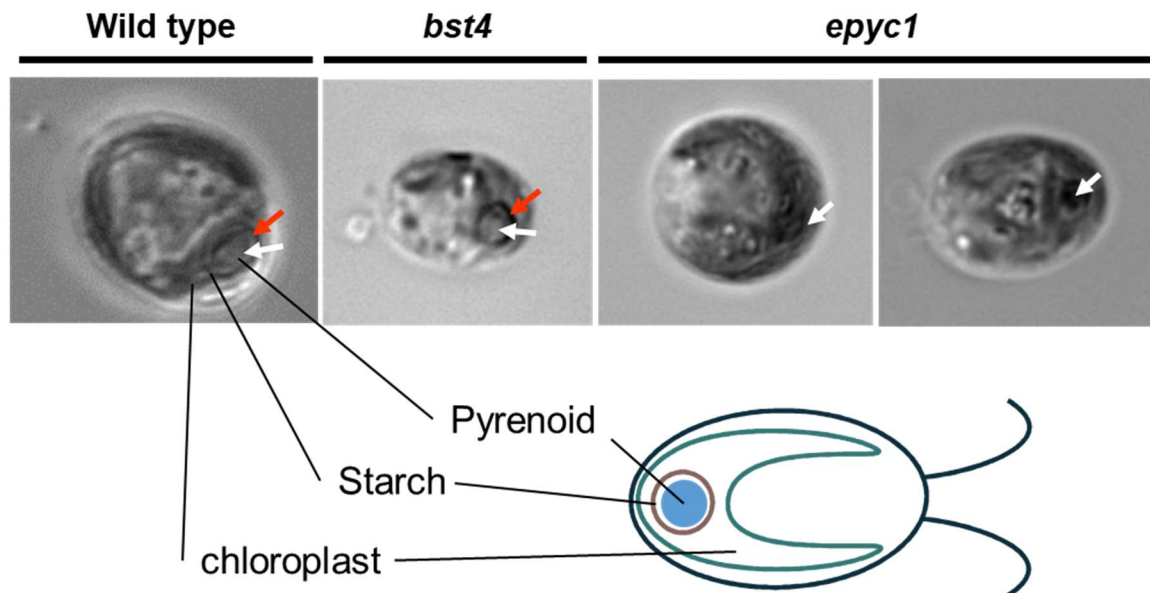

Figure 19. Bright-Field images of the *Chlamydomonas* wild type, *bst4* and *epyc1* strains. Starter cultures of wild type, *bst4* and *epyc1* were grown in TAP medium and were transferred to Tris-minimal medium to induce photosynthesis at least 24 hours prior to imaging. The cells were harvested and resuspended in Lugol's solution diluted with TP for 15 minutes and mounted on glass slides for imaging. The red arrow indicate the starch sheath, and the white arrow indicate the pyrenoid.

For quantitative analysis of the cellular architecture in *Chlamydomonas*, cells must be viewed at a comparable orientation to reduce bias due to the cell section angle. This was achieved by identifying cells that represent the longitudinal mid-section. Cells sectioned this way are likely to exhibit three distinct organelles simultaneously, including the electron-dense pyrenoid (Fig. 20a; red arrow), nucleus (Fig.20a; black arrow) and basal body (Fig. 20a; White arrow) which connects to the flagella.
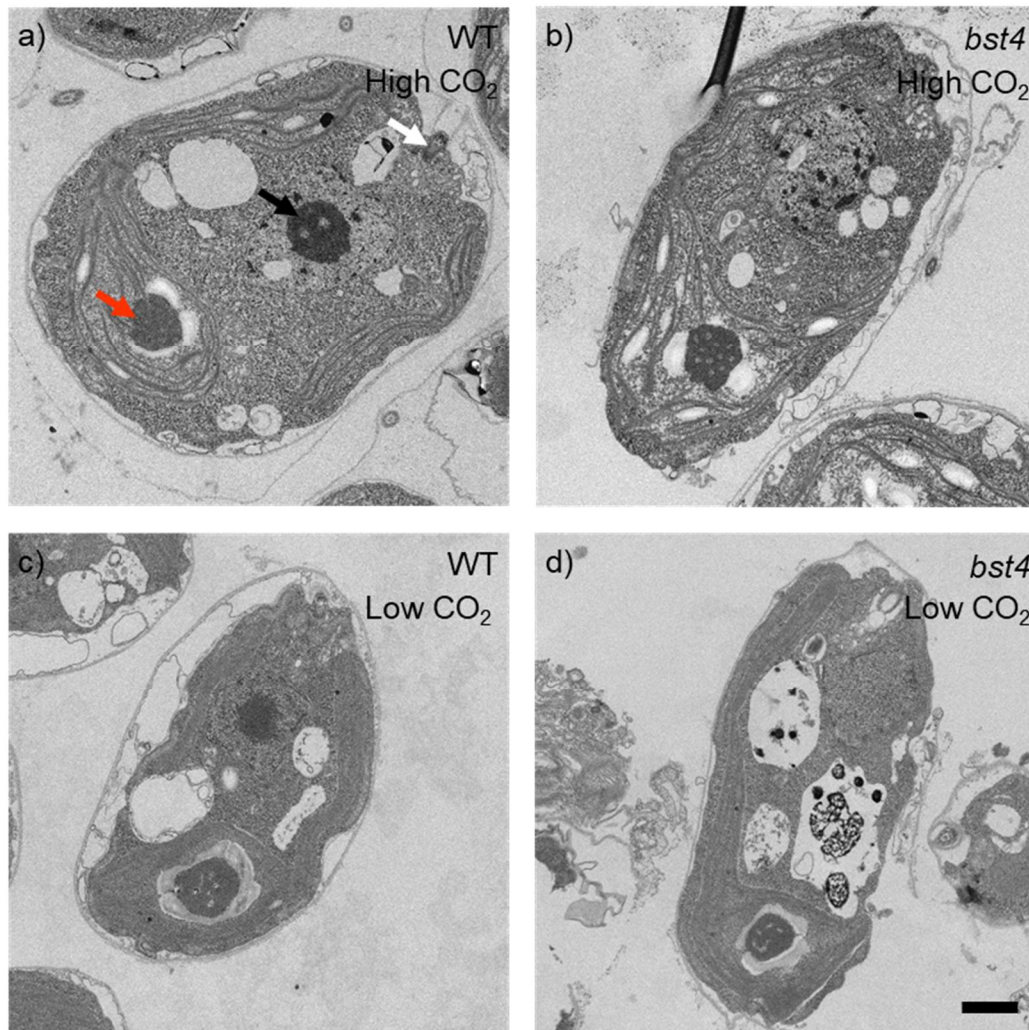
Figure 20. Representative TEM micrographs of wild type and *bst4* strain. Wild type (a, c) and *bst4* (b, d) were acclimated to High and Low CO_2 conditions. Comparable cross-section of cells were indicated by the presence of the pyrenoid (red arrow), nucleus (black arrow) and basal body (white arrow). Scale bar represents 1μm. WT – Wild type.

Analysis of the electron micrographs collected showed that wild type cells exhibit clear CCM-related structural changes. The thickening of starch sheath along with disappearance of free starch granules in the chloroplast can be clearly observed in the low CO_2 acclimated cells (Fig 20) when compared to high CO_2 acclimated cells. Additionally, the pyrenoid size, as indicated by the ratio of pyrenoid area to cell area (Pa:Ca), was shown to increase from 2.5±0.12 at high CO_2 acclimated condition to 3.50 ± 0.12 for low CO_2 acclimated condition (Fig. 21a, closed). Consistent with wild type, *bst4* strains showed similar increase in the Pa:Ca where it increases from 2.55 ± 0.135 to 3.22 ± 0.256 when transferred from high to low CO_2 condition (Fig. 21b; open). The Pa:Ca between wild type and *bst4* strains were not different in low CO_2 condition.

Interestingly, despite exhibiting similar pyrenoid sizes on average, the variability of Pa:Ca is much higher in *bst4* than in wild type (Figure. 21a,c). The recorded standard deviation of data collected from *bst4* strains has reached 1.15 (n=50) in comparison to 0.62 in wild type (n=41).
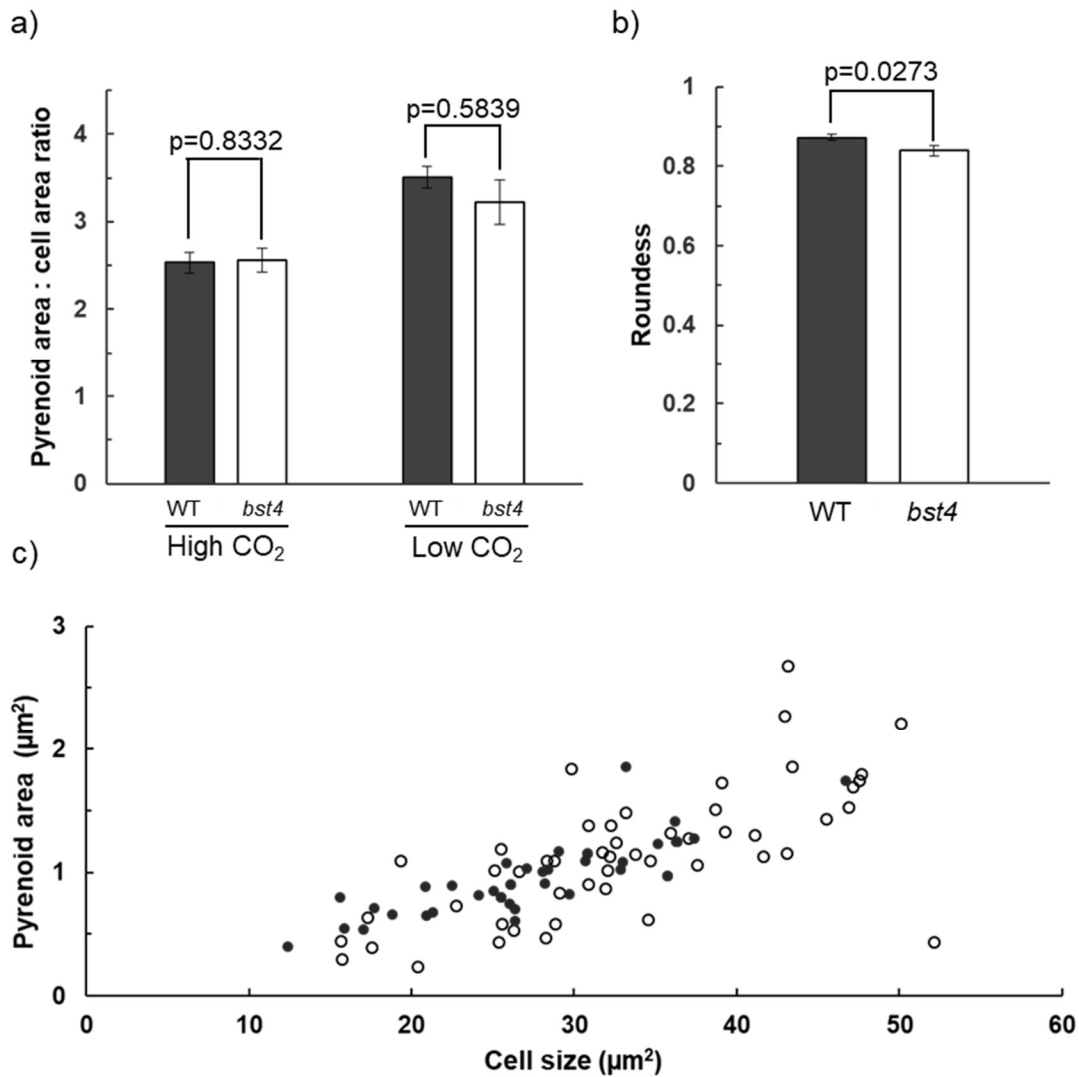

Figure 21. The pyrenoid of *bst4* strains at high and low CO_2 acclimation state. a) The pyrenoid area to cell area ratio of wild type (closed) and *bst4* (open) strains at high and low CO_2 condition. Each bar represents the mean value ± Standard Error (n=40–50), data between wild type and *bst4* strains were tested in two sample T-test and the p-values are displayed above the bars. b) The calculated circularity of pyrenoid in the wild type and *bst4* in the low CO_2 condition c) The pyrenoid area at low CO_2 condition plotted against cell sizes.

Thylakoids in higher plants are known to undergo re-organisation in response to changes in light condition. This is evident by the apparent increase in size and stacking efficiency of grana lamella in higher plants when switched from a dark to a light condition (Pribil *et al.,* 2014; Wood *et al.,* 2018). Despite difference in thylakoid ultrastructure, *Chlamydomonas* was also found to exhibit similarly light-driven changes in thylakoid where the stacking

efficiencies increases upon high light (Polukhina *et al.,* 2016). However, no thylakoid structural change has been found between cells grown in high CO_2 and low CO_2 condition suggesting that thylakoid restructuring is not required in CCM functioning. An Arabidopsis bestrophin-like protein AtVCCN1 (previously known as AtBest1) were found to alter thylakoid ultrastructure if absent (Herdean *et al.,* 2016). To explore whether *bst4* exhibit similar thylakoid structural alteration, the thylakoid stacking efficiencies and the length of each thylakoids between *bst4* and wild type were compared. Interestingly, no observable difference was found between the length and stacking efficiencies of the two strains. (Fig. 22).
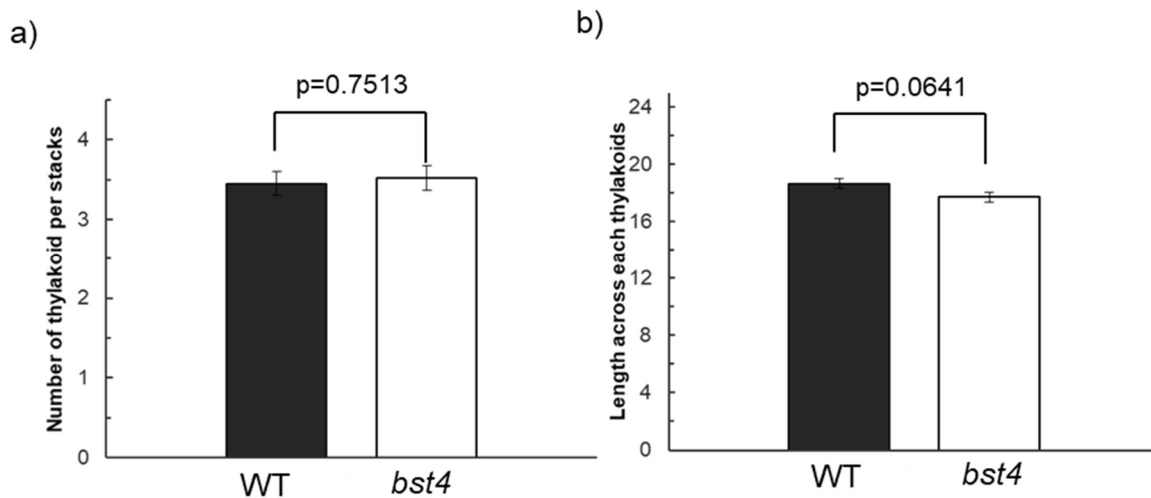

Figure 22. Thylakoid stacking characteristics of wild type and *bst4.* a) The numbers of thylakoid found in each thylakoid stacks. b) The length of each thylakoid stacks recorded. The high and low CO_2 acclimated Wild type (Black) and *bst4* (White) was grown as previously mentioned.

Discussion

Newly identified CCM mutants give novel insights to the Chlamydomonas CCM

In the present work, novel mutants exhibiting a high-CO_2 requiring phenotypes, suggesting possible defects in their CCM, were identified. These mutants were previously identified as interactors of known CCM components and their further characterisation will likely shed light on the mechanistic details of the CCM. Among the identified high-CO_2 requiring mutants, 8 are potentially deficient in Rubisco-interacting proteins. Annotations of these rubisco-interacting proteins were widely varied and not limited to the traditional carbon-fixation role, such as Cre13.g575800 which was annotated as indole-3-glycerol-phosphate synthase which is a tryptophan and auxin precursor in higher plants (Ouyang *et al.,* 2000), Cre06.g271850 which contains an ABC-F type transporter domain as well as Cre08.g373450, also known as starch binding enzyme 4 (SBE4). SBE4 is particularly interesting, as a starch branching enzyme, and due to its high-CO_2 requiring phenotype, it is likely that starch biosynthesis is involved in the *Chlamydomonas* CCM. This is contrary to previous evidence which found that a starch-less mutant of *Chlamydomonas* and a closely related pyrenoid containing green algae, *Chlorella pyrenoidosa* exhibit no change in CCM activity relative to wild type despite the complete loss of starch sheath. (Villarejo *et al.,* 1996; del Pino Plumed 1996). In the pyrenoid, there are pyrenoid minitubules that were similar to invagination of thylakoid tubules connecting the chloroplast stroma and pyrenoid matrix (Engel *et al.,* 2015). These pyrenoid minitubules first emerge in close proximity to the starch sheath and are crucial to the metabolite fluxes between pyrenoid matrix and chloroplast stroma, therefore the formation and expansion of starch sheath must be tightly regulated to prevent blockage. Further efforts to characterise this mutants might allow a better understanding of the relationship between starch plate development and pyrenoid minitubule formation.

BST4 contributes to operation of the CCM at low CO_2

From the CCM screen we identified *bst4* to exhibit a growth defect that is exacerbated at high pH under low CO_2 conditions. The high pH used in the medium tilts the equilibrium of $HCO_3^-:CO_2$ with a calculated one hundred fold increase in $HCO_3^-:CO_2$ at pH 8.4 compared to pH 7. This suggests that not only does the *bst4* mutant exhibit a high-CO_2 requiring phenotype, but also hints that its growth deficiency might be associated with HCO_3^- transport processes. Bestrophins are widely conserved proteins occurring in many organisms and

have been implicated as the primary cause of the Best Vitelliform Macular Dystrophy (BVMD), a degenerative eye disease, in humans (Xiao *et al.,* 2010). Bestrophins were first proposed to act as Cl^- ion channels in human retinal pigment epithelium cells and the disruption of this chloride flow is the primary cause of BVMD. However, a study investigating mouse bestrophin showed that they are capable of mediating HCO_3^- transport activity to a similar extent to Cl^-. (Qu and Hartzell *et al.,* 2008). The identified HCO_3^- transport activity prompted questions in whether *Chlamydomonas* bestrophins mediate HCO_3^- and whether they can act as the enigmatic HCO_3^- in the thylakoid membranes.

To confirm the involvement of BST4 in the CCM, the *bst4* mutant line was grown in liquid under low CO_2 conditions. We found that the *bst4* strain does not exhibit any growth difference from wild type when grown under low CO_2 at a low light intensity of 50 µmols photons m^{-2} s^{-1}. However, increasing the light intensity to 400 µmols photons m^{-2} s^{-1} significantly alters their growth rate. At this high light intensity, *bst4* exhibits a clear reduced growth rate (Fig 8). The apparent difference in growth phenotype corresponding to the light condition used in growth assays can be reasoned due to sub-optimally operating photosynthesis masking any deficiency in the carbon-fixation pathway. As the saturating light intensity *Chlamydomonas* have been previously reported to be at 500 µmol photons m^{-2} s^{-1} (Kirst *et al.,* 2012; Perrine *et al.,* 2012), the lack of discernible difference between growth rate was likely the result of minimal requirement in carbon fixation at low light intensity. Similarly, light-dependent CCM related proteins have also been reported, such as in HLA3 where gene expression is activated by both action of limiting CO_2 and strong light condition (~1200 uE) which further indicates that high light intensity possibly drives a strong requirement for carbon fixation in order to compensate for energy generated by light reactions (Im and Grossman 2002).

Aside from the low CO_2 growth phenotype, *bst4* also showed physiological defects under low CO_2 conditions that support the theory that BST4 is involved in the CCM. We demonstrated the *bst4* mutant exhibit lowered C_i affinity in comparison to wild type under the low CO_2 acclimation state (Table 3). As external C_i concentration approaches saturation (>500 µM), the difference between O_2 evolution rates between strains is minimal at both acclimation states showing that *bst4* exhibits a similar photosynthetic capability to wild type under non-limiting C_i conditions (Fig. 16). This capability is further exemplified by the similar chlorophyll content and chlorophyll a/b ratio measured (Fig. 17) which demonstrate that the light-dependent reaction in *bst4* is unlikely to be impaired. The low CO_2 acclimated specific photosynthetic defect detected therefore implicates its involvement in the CCM. As opposed to previous discoveries which found LCIA's contribution to O_2 evolution to be most

pronounced at the very low CO_2 range (Wang and Spalding 2014), the reduced O_2 evolution found in *bst4* is most pronounced at the low CO_2 range instead (Fig. 16c; 10 μM–50 μM $[C_i]$). This suggests that the BST4 protein is not only involved in the CCM, but also has preferential importance at the low CO_2 acclimation state.

The bestrophin proteins are structurally similar to their Cl^-/HCO_3^- transporting homologs.

Comparison of the *Chlamydomonas* bestrophin protein sequences showed that they are highly homologous in the annotated bestrophin domain (Fig. 11) but possess a highly diverse C-terminal tail that is similar to that previously reported of human bestrophins (Tsunenari *et al.,* 2003). Additionally, the conservation of the 4 predicted transmembrane domains and their corresponding spacing were highly reminiscent of their mammal and bacterial counterparts despite the poor sequence identity conservation between themselves (<18%).

Previous reports have demonstrated that ion selectivity and permeation in bestrophins are partly influenced by the critical residues that are located at the channel pore-lining possibly through a size-restriction mechanism or electrostatic potential (Yang *et al.,* 2014, Qu *et al.,* 2006). Using homology modelling, we obtained structural models of BST1–4 proteins using the *Klebsiella pneumonia* bestrophin template (PDB: 4WD8). Analysis of the pore-lining residues in the modelled structures of BST1–4 revealed that these residues generally correspond to alanine, leucine and phenylalanine (Fig. 12a). The last residue leading to the inner cavity region of Bestrophin channel (Fig 12a) was found to be conserved as phenylalanine in all the bestrophins examined. This residue has been proposed to exhibit a weak positive electric potential due to its aromatic ring which aids in anion-transport (Vaisey *et al.,* 2016). This was in agreement with the electrostatic potential calculation using the Poisson-Boltzman equation, which suggested that the pore-lining of the channel exhibits a positive electrostatic potential (Fig. 12c), and was also consistent to the electrostatic potential calculated on the modelled structure of human bestrophins (Yang et al, 2014). While homology modelling of proteins is prone to error as it relies heavily on the resolution of template used during modelling where poor sequence conservation might lead to poor fitting. The local Q-mean scores, which assess structural model quality, has remained high at the pore linings and the overall structure for all modelled structures (Fig. 12d). This suggests the modelled structures adhere well to the geometric restrains that stems from the residue torsion angle and solvation energy (Benkert *et al.,* 2008). Along with the overlap of the predicted secondary structure found between Kpbest, and BST1–4 (Fig.11), the obtained

structure model and sequence analysis suggests that the BST1–4 are likely structural homologs to the Cl⁻/HCO₃⁻ transporting bestrophins.

The distribution of the Chlamydomonas *bestrophins*

Expression of the chimeric BST1–4 and YFP construct in wild type strains demonstrate that BST1–4 proteins were localised to the chloroplast, more specifically, BST1–3 were found at the thylakoids aggregating around the pyrenoid whereas BST4 was found at the pyrenoid tubules. The localisation pattern of the bestrophins support their hypothetical role as HCO_3^- transporters. As the presence of BST1–3 preferentially localised at the thylakoids surrounding pyrenoid, a relatively high proportion of HCO_3^- can be shuttled to the pyrenoid central localised CAH3 via a short diffusion distance. This short diffusion distance minimised the duration in which HCO_3^- was exposed to the acidity in thylakoid lumen, such that leakage of CO_2 can be reduced. (Fig. 23). Similarly, the dehydration of HCO_3^- by CAH3 should create a HCO_3^- sink which drives the movement of HCO_3^-. The localisation of BST1–3 were therefore prime location for HCO_3^- transport.
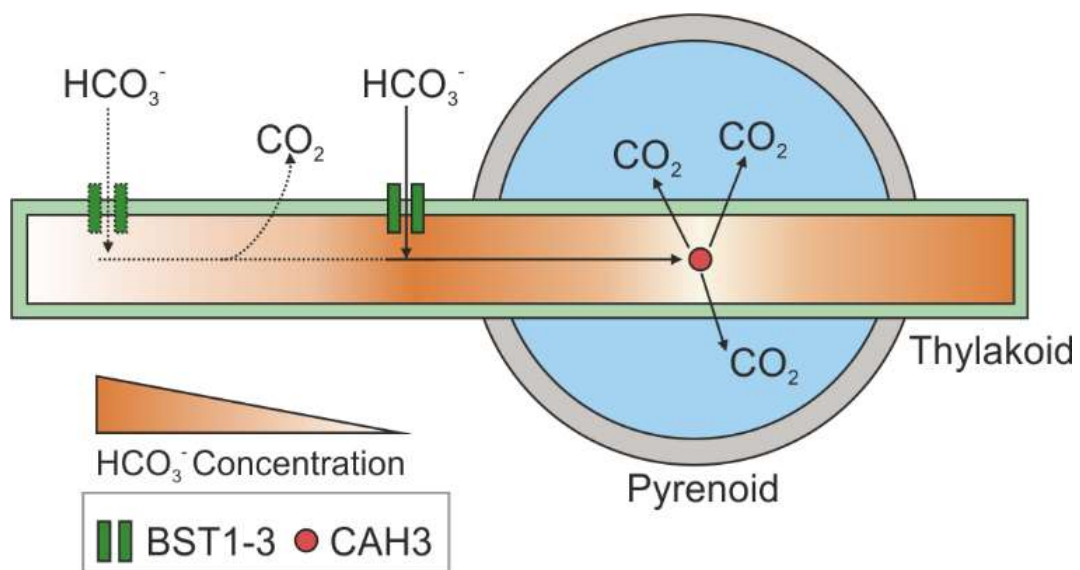

Figure 23. Potential role of BST1–3. HCO_3^- transported from the bestrophin located further from pyrenoid (dashed rectangle) experience long diffusion distance from CAH3 and were likely converted to CO_2 by the acidity of thylakoid lumen. The localisation of BST1–3 (solid rectangle) enriched surrounding pyrenoid represents a strategic position which allow short-diffusion distance between HCO_3^- sink.

Since known CCM components such as CAS and LCIB proteins have been shown to re-localises in response to CCM induction (Yamano *et al.,* 2010; Wang *et al.,* 2016), we investigated whether BST4 re-localises after dark incubation which suppresses the CCM. Interestingly, we saw no re-localisation even after incubation in the dark for 50 minutes. It

might be argued that the intermittent laser during the imaging period possibly disturbs the re-localisation since it stimulates photosynthesis. However, the short laser pulse used (514nm) is on the relatively low absorption region over the *Chlamydomonas* absorption spectrum (Mooji *et al.,* 2016), such that the short pulse is unlikely to sufficiently induce the CCM. Additionally, the re-localisation of the LCIB-LCIC complex in dark-incubated cells was also shown to occur within 1 hour, which was consistent to the time-scale used here. Hence, we conclude that BST4 does not re-localise in response to the CCM induction state

BST4 potentially has a dual function in the Chlamydomoas CCM

The BST4 amino acid sequence contains a bestrophin domain and a potential rubisco binding domain. These domains suggests that BST4 potentially exhibits dual function as a HCO_3^- transport component and pyrenoid-interacting protein. In this work, BST4 was implicated to participate in CCM operation. With its similarity to the HCO_3^- transporting bestrophins, we proposed that BST4 functions as a HCO_3^- channel which recycles the free HCO_3^- at the pyrenoid matrix. As shown by a Cryo-EM study of *Chlamydomonas*, the pyrenoid matrix is continuous with the chloroplast stroma through a connection lead by the pyrenoid minitubules (Engel *et al.,* 2015). The continuous environment and dynamic nature of the pyrenoid suggests that the pyrenoid likely exhibits an alkaline pH environment. Indeed, a recent study determined that the pH environment in the pyrenoid matrix would rise to >pH 8.2 under light, which was consistent with that of the chloroplast stroma under light (Freeman-Rosenzweig 2017). The alkaline environment in the pyrenoid matrix poses a problem during the CCM, as the CCM drives the rapid release of CO_2 at the pyrenoid matrix to saturate Rubisco, likely leaving a proportion of CO_2 unfixed. This unfixed CO_2 will be favourably converted to HCO_3^- in the aforementioned alkaline environment of the pyrenoid matrix. The conversion creates a local concentration spike of HCO_3 at the pyrenoid matrix that unless recycled, will disperse from the pyrenoid resulting in a 'leaky' CCM. Located at the centre of the pyrenoid, BST4 is primed to deliver this locally concentrated HCO_3^- back to the thylakoid lumen for dehydration, hence forming a pH-dependent recycling pathway (Fig. 25). This idea is supported by the O_2 evolution results. As the contribution of BST4 in O_2 evolution in low CO_2 acclimated state which is calculated by subtracting *bst4* O_2 evolution rate from that of wild type showed the BST4 predominantly contribute in the low C_i range (<50 µM; Fig. 16c). In the low C_i condition, the leakage will critically impact the CCM efficiency since it leads to the loss of energy that were used to actively concentrate C_i as well the loss of accumulated C_i through passive diffusion. As opposed to a high C_i condition where this loss of C_i from CCM can be compensated by the high external C_i which drives

passive diffusion. Indeed, the contribution of *bst4* reduced once C_i concentration approaches saturation (>500 µM).

Similarly, the BST1–3 might also participate in a HCO_3^- recycling mechanism due to their interaction with the LCIB-LCIC complex (Mackinder *et al.,* 2017). The LCIB-LCIC complex has been hypothesised to participate in a CO_2 recapture system by rehydrating the leaked CO_2 to HCO_3^- at the pyrenoid periphery. Since BST1–3 were shown to be enriched at the thylakoids surrounding the pyrenoid periphery (Fig. 14), this can allow quick re-shuttling of HCO_3^- to the thylakoid lumen, therefore constituting a HCO_3^- recycling pathway.

In comparison to the CCM operating cyanobacteria where CO_2 release is directly within the gas-impermeable carboxysomes to avoid potential leakage (Long *et al.,* 2018), the *Chlamydomonas* pyrenoid is dynamic with mixing and is continuous with the chloroplast stroma (Freeman-Rosenzweigh 2017; Engel *et al.,* 2015). While encapsulated by a starch sheath, there are apparent openings where thylakoid tubules penetrate, that would enable CO_2 leakage, reducing CCM-operating efficiency. The presence of a scavenger/recycling system surrounding the pyrenoid provides a logical solution to recover leaked CO_2. Rapidly released CO_2 delivered by the CCM, lost either as CO_2 or HCO_3^- can be recycled through the proposed recycling mechanism provided by the strategically localised bestrophin family.
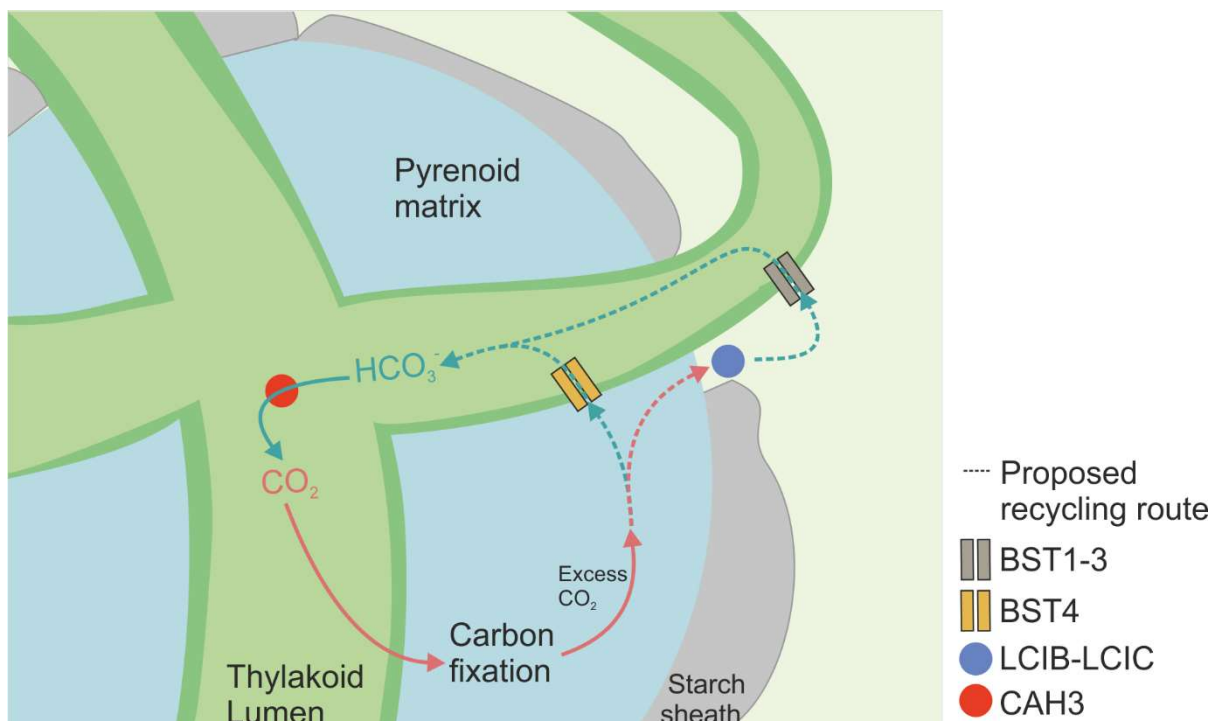

Figure 24. The potential HCO_3^- recycling pathway mediated by bestrophin proteins in *Chlamydomonas*. CO_2 released by the accumulated HCO_3^- is used predominantly by Rubisco in the pyrenoid for carbon fixation. As the released CO_2 saturates Rubisco, a proportion of CO_2 is converted

to HCO_3^- due to the alkaline environment, this is recycled by the BST4 protein and re-shuttled to thylakoid lumen for dehydration. The remaining proportion of CO_2 is captured by the LCIB-LCIC complex that situates at the pyrenoid-periphery. LCIB-LCIC complex rehydrate the leaked CO_2 and allow HCO_3^- to reach the thylakoid lumen via BST1–3.

Despite the similarity between residue profile and secondary structure of BST4 and EPYC1, the TEM analysis of *bst4* strains showed that the pyrenoid sizes does not differ from wild type. When expressed as a ratio of pyrenoid size to cell size (Pa:Ca), the wild type pyrenoids have consistently remained close to a ratio of 3.5 in all cell sizes measured. In *bst4* however, the pyrenoid size appeared significantly more variable, and the shape of *bst4*'s pyrenoid appeared less rounded (Fig. 21). The lack of consistent Pa:Ca in *bst4* could stem from a weak association of pyrenoid to thylakoid membrane. While the pyrenoid assembles at the thylakoid knot, neither Rubisco nor EPYC1 contain any transmembrane domains that allow the pyrenoid to be anchored to the thylakoid knot. Known to interact with Rubisco through a proteomics study (Mackinder *et al.,* 2017), the membrane-bound BST4 could enable the pyrenoid to adhere to the thylakoid knot via interaction of Rubisco and BST4's disordered tail. Nevertheless, the subtlety of *bst4* phenotype preclude BST4 functioning as the sole operator that anchors the pyrenoid to the thylakoid. It is highly like that multiple different proteins engage in the liquid-behaviour in *Chlamydomonas* pyrenoid, as Mackinder *et al* (2016) showed that a residual amount of pyrenoid assembles at the thylakoids in *epyc1* despite the lack of EPYC1 protein. However, it is also possible that BST4's disordered tail exhibit no structural role to the anchoring of pyrenoid to the thylakoid knot. Since BST4's localisation differs from BST1, 2 and 3, the EPYC1-like C-terminal of BST4 might act as a localising signal instead. This can allow BST4 to be localised to the thylakoid knot rather than the thylakoid membrane despite the high degree of homology shared between BST4 and the other bestrophin sequences. Nevertheless, the *bst4* phenotypes were subtle and difficult to interpret in the *in vivo* system. The use of heterologous systems such as Yeast-2-hybrid screening or an *in vitro* systems such as the one used in Wunder *et al.,* (2018) where the binding ability of BST4 to Rubisco can be directly assessed will greatly benefit the characterisation of BST4's disordered tail.

Under light, the photosynthetic electron transfer generates a proton motive force (PMF) that is used to drive ATP-synthesis. The PMF can partitioned into proton gradient (ΔpH) and membrane potential (ΔΨ) across the thylakoid membrane. Under steady state, the ΔpH is the predominant component of PMF while ΔΨ is quickly dissipated to avoid photoinhibition (Johnson and Ruban 2014). A bestrophin-like protein in *Arabidopsis thaliana,* termed AtVCCN1 has recently been shown to function as a voltage-gated Cl^- channel located at the thylakoid membrane. It was suggested that the Cl^- channel allows rapid dissipation of ΔΨ as

PMF builds up under light (Herdean *et al.,* 2016). Alongside with the increased partitioning of PMF into $\Delta\Psi$, they observed increased stacking efficiency of thylakoids in the knockout lines likely due to the ion-imbalance in the thylakoid lumen. The change in thylakoid structure was also seen in a knock-out of a paralogous gene, which resulted in the thylakoid lumen thickness being almost double from that of wild type (Duan *et al.,* 2016). In *bst4*, we found that the thylakoid structure does not differ from that of wild type at low CO_2. The stacking efficiency of *bst4* and wild type similarly contain approximately 3.4–3.5 thylakoids per stack and that the thylakoid thickness was calculated to be approximately 17–18 nm per thylakoids (Fig. 22). While *Chlamydomonas* thylakoid does not segregate to grana and stroma lamella, the lack of thylakoid structural changes suggests that BST4 does not function similarly to its higher plant counterparts. This is also supported by its localisation at the thylakoid membrane traversing the pyrenoid matrix. As despite the highly dynamic nature of the pyrenoid, BST4 lack immediate contact to the stroma space, this does not support the rapid Cl^- influx into thylakoid lumen required to dissipating $\Delta\Psi$ under light.

In conclusion, this work presents the discovery of multiple additional proteins involved in the CCM. More prominently, the localisation of novel bestrophin proteins BST1–4, the BST4 deficient strain exhibit a clear defect in the CCM. From the peptide analysis of the bestrophin proteins, we proposed that the BST4 potentially functions as a HCO_3^- channel at the thylakoid membrane which allows pH dependent recycling of HCO_3^- in the pyrenoid under light. It is important for regulating pyrenoid assembly possibly through its C-terminal interactions.

Supplementary materials
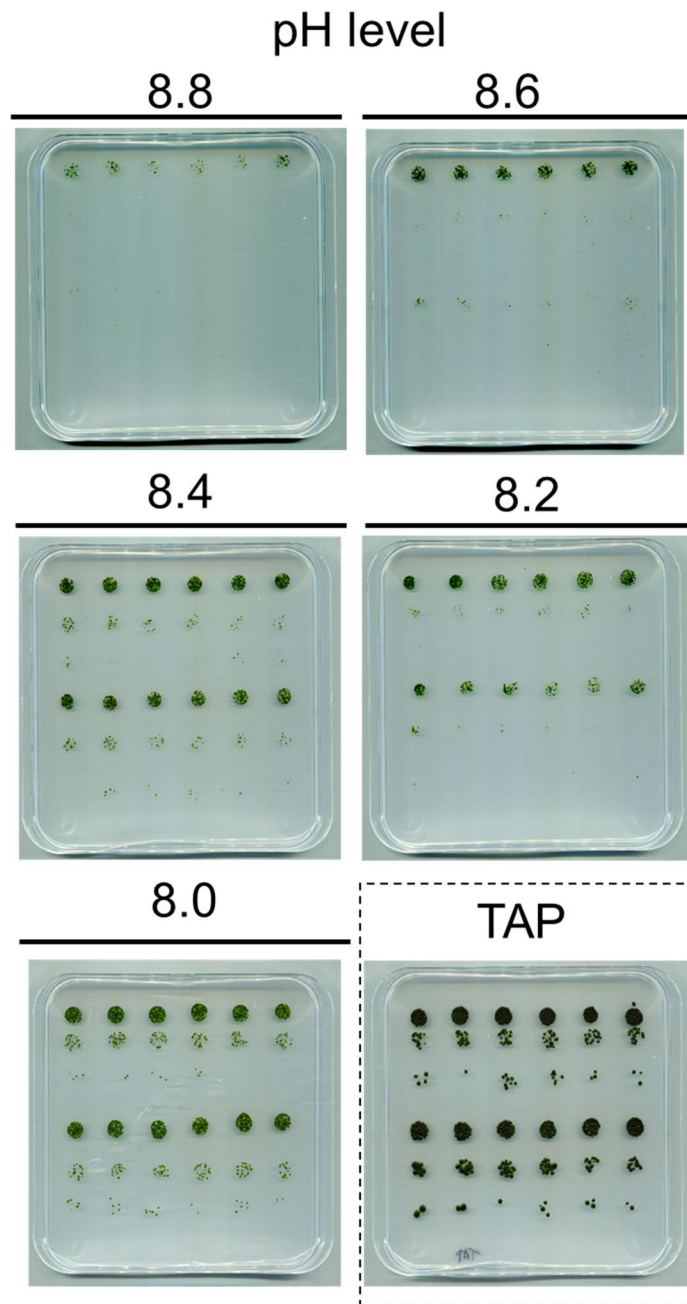
Supplementary Figure 1. Full plates of pH assay. The corresponding pH condition of each plate is indicated above the plate. Cultures spotted on TAP plates were used as a loading control and shown on the dashed region.
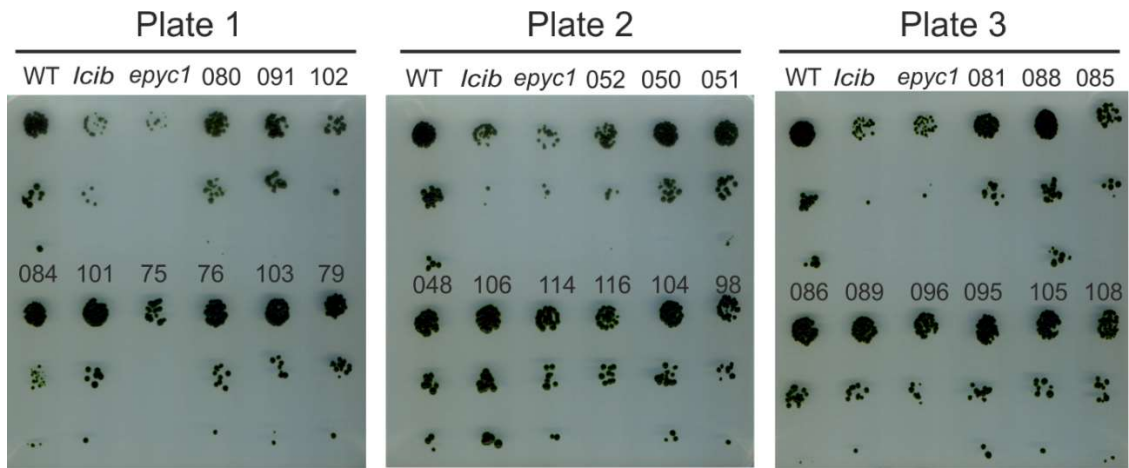
Supplementary Figure 2. TAP plates of CCM mutant screen. Cell suspension were spotted on TAP plate as loading control for the CCM screening. The strain number is denoted on top of each spots.

List of abbreviations

1. TAP: Tris-acetate-phosphate medium
2. TP: Tris-minimal medium
3. BVMD: Best Vitelliform Macular Dystrophy
4. C_i: Inorganic carbon
5. CCM: Carbon Concentrating Mechanism
6. *Chlamydomonas*: *Chlamydomonas reinhardtii*
7. CO_2: Carbon dioxide
8. Cl^-: Chloride ion
9. CO_2: Carbon dioxide
10. Cryo-EM: Cryogenic Electron Microscopy
11. HCO_3^-: Bicarbonate ion
12. TEM: Transmission Electron Microscopy
13. PSI: Photosystem 1
14. PSII: Photosystem 2
15. Pa:Ca Pyrenoid area: Cell area
16. RuBP: Ribulose-Bisphosphate

References

1. Altschul SF, Gish W, Miller W, Myers EW, Lipman DJ, Basic local alignment search tool, *J Mol Biol*, 1990;215(3): 403-410.

2. Amoroso G, Sültemeyer D, Thyssen C, Fock HP. Uptake of HCO_3^- and CO_2 in Cells and Chloroplasts from the Microalgae *Chlamydomonas reinhardtii* and *Dunaliella tertiolecta*. *Plant Physiol*. 1998;116(1):193-201.

3. Atkinson N, Feike D, Mackinder LC, Meyer TM, Griffith H, Konikas MC, Smith AM, McCormick AJ. Introducing an algal carbon-concentrating mechanism into higher plants: location and incorporation of key components. *Plant Biotechnol J*. 2016;14(5):1302-15.

4. Badger MR, Kaplan A, Berry JA. Internal Inorganic Carbon Pool of *Chlamydomonas reinhardtii*: Evidence for a Carbon Dioxide Concentration Mechanism. *Plant Physiol*. 1980;66(3):407-413.

5. Benkert P, Tosatto SCE, Schomburg D. QMEAN: A comprehensive scoring function for model quality assessment. *Proteins*, 2008;71(1):261-277.

6. Blanco-Rivero A, Shutova T, Román MJ, Villarejo A, Martinez F (2012) Phosphorylation Controls the Localization and Activation of the Lumenal Carbonic Anhydrase in *Chlamydomonas reinhardtii*. *PLOS ONE*, 2012;7(11):e49063.

7. Borkhsenious ON, Mason CB, Moroney JV. The Intracellular Localization of Ribulose-1,5-Bisphosphate Carboxylase/Oxygenase in *Chlamydomonas reinhardtii*. *Plant Physiol*. 1998; 116(4):1585-1591.

8. Brueggeman AJ, Gangadharaiah DS, Cserhati MF, Casero D, Weeks DP, Ladunga I. Activation of the carbon concentrating mechanism by CO_2 deprivation coincides with massive transcriptional restructuring in *Chlamydomonas reinhardtii*. *Plant Cell*. 2012;24(5):1860-75.

9. Caspari OD, Meyer MT, Tolleter D, Wittkopp TM, Cunniffe NJ, Lawson T, Grossman AR, Griffiths H. Pyrenoid loss in *Chlamydomonas reinhardtii* causes limitations in CO_2 supply, but not thylakoid operating efficiency. *J Exp Bot*. 2017;68(14):3903-3913.

10. Chien LT, Hartzell HC. Rescue of volume-regulated anion current by bestrophin mutants with altered charge selectivity. *J Gen Physiol*. 2008;132(5):537-46.

11. Chou TH. Crystal Structure of a Low CO_2-Inducible Protein, LCI1 in *Chlamydomonas reinhardtii*, *Biophysical Journal*. 2017;112(3): 22a, Supplement 1.

12. Covshoff S, Hibberd JM. Integrating C4 photosynthesis into C3 crops to increase yield potential. *Curr. Opin. Biotechnol.* 2012;23: 209-214.

13. Cruz JA, Sacksteder CA, Kanazawa A, Kramer DM. Contribution of Electric Field ($\Delta\psi$) to Steady-State Transthylakoid Proton Motive Force (pmf) in Vitro and in Vivo. Control of pmf Parsing into $\Delta\psi$ and ΔpH by Ionic Strength, *Biochemistry*, 2001;40(5):1226-1237.

14. De Bossoreille de Ribou S, Douam F, Hamant O, Frohlich MW. Plant science and agricultural productivity: Why are we hitting the yield ceiling? *Plant science*, 2013;210:159-176

15. Del Pino Plumed M, Villarejo A, de los Róos A, Garcia-Reina G, Ranazabiv Z The CO_2-concentrating mechanism in a starchless mutant of the green unicellular alga *Chlorella pyrenoidosa*. *Planta*, 1996; 200(1):28-31.

16. Dickson VK, Pedi L, Long SB. Structure and insights into the function of a Ca^{2+}-activated Cl^- channel. *Nature*. 2014;516(7530):213-218.

17. Duan Z, Kong F, Zhang L, Li W, Zhang J, Peng L. A bestrophin-like protein modulates the proton motive force across the thylakoid membrane in Arabidopsis. *J Integr Plant Biol.* 2016;58(10): 848–858

18. Duanmu D, Miller AR, Horken KM, Weeks DP, Spalding MH. Knockdown of limiting-CO_2–induced gene HLA3 decreases HCO_3^- transport and photosynthetic C_i affinity in *Chlamydomonas reinhardtii*. *Proc Nat Acad Sci USA*. 2009;106(14):5990-5995.

19. Duanmu D, Wang Y, Spalding MH. Thylakoid Lumen Carbonic Anhydrase (CAH3) Mutation Suppresses Air-Dier Phenotype of LCIB Mutant in *Chlamydomonas reinhardtii*. *Plant Physiol*. 2009;149(2):929-937.

20. Edgar RC. MUSCLE: multiple sequence alignment with high accuracy and high throughput. *Nucleic Acids Res.* 2004;32(5):1792-7.

21. Emanuelsson O, Nielsen H, von Heijne G. ChloroP, a neural network-based method for predicting chloroplast transit peptides and their cleavage sites. *Protein Sci*. 1999;8(5):978-984.

22. Engel BD, Schaffer M, Kuhn Cuellar L, Villa E, Plitzko JM, Baumeister W. Native architecture of the *Chlamydomonas* chloroplast revealed by *in situ* cryo-electron tomography. *eELife*. 2015;4:e04889.

23. Fang W, Si Y, Douglass S, Casero D, Merchant S, Pellegrini M, Ladunga I, Liu P, Spalding M. Transcriptome-wide changes in *Chlamydomonas reinhardtii* gene expression regulated by carbon dioxide and the CO2-concentrating mechanism regulator CIA5/CCM1. *Plant Cell.* 2012;24(5):1876-93.

24. Freeman-Rosenqweig ES. Dynamics and liquid-like behaviour of the pyrenoid of the green alga *Chlamydomonas reinhardtii.* Standford University, Doctoral Dissertation 2017.

25. Fujiwara S, Fukuzawa H, Tachiki A, Miyachi S. Structure and differential expression of two genes encoding carbonic anhydrase in *Chlamydomonas reinhardtii*. *Proc Natl Acad Sci USA*. 1990;87(24):9779-83.

26. Fukuzawa H, Miura K, Ishizaki K, Kuchi KI, Saito T, Kohinata T, Ohyama K. CCM1, a regulatory gene controlling the induction of a carbon-concentration mechanism in

Chlamydomonas reinhardtii by sensing CO_2 availability. *Proc Nat Acad Sci USA*. 2001;98(9):5347-5352.

27. Furbank RT. Walking the C4 pathway: past, present, and future, *J Exp Bot*. 2016;67(14): 4057-4066

28. Gao H, Wang Y, Fei X, Wright DA, Spalding MH. Expression activation and functional analysis of HLA3, a putative inorganic carbon transporter in *Chlamydomonas reinhardtii*. *Plant J.* 2015;82: 1-11.

29. Gorman DS, Levine RP. Cytochrome f and plastocyanin: their sequence in the photosynthetic electron transport chain of *Chlamydomonas reinhardi. Proc Natl Acad Sci USA*. 1965;54(6):1665-9.

30. Hanson DT, Franklin LA, Samuelsson G, Badger MR. The *Chlamydomonas reinhardtii cia3* mutant lacking a thylakoid lumen-localized carbonic anhydrase is limited by CO_2 supply to rubisco and not photosystem II function in vivo. *Plant Physiol.* 2003;132(4):2267-75.

31. Heger A, Holm L. Rapid automatic detection and alignment of repeats in protein sequences. *Proteins*. 2000;41(2):224-237.

32. Herdean A, Teardo E, Nilsson A, Pfeil B, Johansson ON, Ünnep R, Nagy G, Zsiros O, Dana S, Solymosi K, Garab G, Szabó I, Spetea C, Lundin B. A voltage-dependent chloride channel fine-tunes photosynthesis in plants. *Nat Commun.* 2016;7:11654.

33. Hirooka S, Hirose Yuu, Kanesaki Y, Higuchi S, Fujiwara T, Era A, Ohbayashi R, Uzuka A, Nozaki H, Yoshikawa H, Miyagishima SY. Draft genome of an acidophilic green alga *Proc Nat Acad Sci USA*. 2017;114(39):E8304-E8313.

34. Im CS, Grossman AR. Identification and regulation of high light-induced genes in *Chlamydomonas reinhardtii. The Plant J.* 2002;30(3):301-313.

35. Jin S, Sun J, Wunder T, Tang D, Cousins AB, Sze SK, Mueller-Cajar O, Gao YG. Structural insights into the LCIB protein family reveals a new group of β-carbonic anhydrases. *Proc Natl Acad Sci USA*. 2016;113(51):14716-14721.

36. Jones DT. Protein secondary structure prediction based on position-specific scoring matrices. *J. Mol. Biol.* 1999; 292(2): 195-202.

37. Johnson MP, Ruban AV. Rethinking the existence of a steady-state component of the proton motive force across the plant thylakoid membrane. *Photosynth Res.* 119:233–242

38. Jungnick N, Ma Y, Mukherjee B, Cronan JC, Speed DJ, Laborde SM, Longstreth DJ, Moroney JV. The carbon concentrating mechanism in *Chlamydomonas reinhardtii*: finding the missing pieces. *Photosynth Res.* 2014;121(2-3):159-173.

39. Karlsson J, Clarke AK, Chen ZY, et al. A novel alpha-type carbonic anhydrase associated with the thylakoid membrane in *Chlamydomonas reinhardtii* is required for growth at ambient CO_2. *The EMBO Journal*. 1998;17(5):1208-1216.

40. Kapoor K, Duff MR, Upadhyay A, Bucci JC, Saxton SM, Hinde RJ, Howell EE, Baudry J. Highly Dynamic Anion–Quadrupole Networks in Proteins. *Biochemistry* 2016;55(43):6056-6069.

41. Kirst H, Garcia-Cerdan JG, Zurbriggen A, Ruehle T, Melis A. Truncated Photosystem Chlorophyll Antenna Size in the Green Microalga *Chlamydomonas reinhardtii* upon Deletion of the TLA3-CpSRP43 Gene. *Plant Physiol*. 2012;160(4):2251-2260.

42. Korobchevskaya K, Lagerholm BC, Colin-York H, Fritzsche M. Exploring the Potential of Airyscan Microscopy for Live Cell Imaging. *Photonics,* 2017;4(3)41.

43. Kropat J, Hong-Hermesdorf A, Casero D, et al. A revised mineral nutrient supplement increases biomass and growth rate in *Chlamydomonas reinhardtii*. *Plant J*. 2011;66(5):770-80.

44. Kumar S, Stecher G, Li M, Knyaz C, Tamura K. MEGA X: Molecular Evolutionary Genetics Analysis across Computing Platforms. *Mol Biol Evol.* 2018;35(6):1547-1549

45. Li YY, Yu H, Guo ZM, Guo TQ, Tu K, Li YX. Systematic analysis of head-to-head gene organization: evolutionary conservation and potential biological relevance. *PLoS Comput Biol*. 2006;2(7):e74.

46. Li X, Zhang R, Patena W, et al. An Indexed, Mapped Mutant Library Enables Reverse Genetics Studies of Biological Processes in *Chlamydomonas reinhardtii. Plant Cell*. 2016;28(2):367-87.

47. Liebich J, Schäffer A, Burauel P. Structural and functional approach to studying pesticide side effects on specific soil functions. *Environ. Toxicol. Chem.* 2003;22(4):784-790.

48. Linding R, Jensen LJ, Diella F, Bork P, Gibson TJ, Russell RB. Protein Disorder Prediction: Implications for Structural Proteomics. *Structure*, 2003;11(11):1453-1459.

49. Long BM, Hee WY, Sharwood RE, Rae BJ, Kaines S, Lim YL, Nguyen ND, Massey B, Bala S, von Caemmerer S, Badger MR, Price GD. Carboxysome encapsulation of the CO_2-fixing enzyme Rubisco in tobacco chloroplasts. *Nat Commun*. 2018;9(1):3570.

50. Long SP, Marshall-Colon A, Zhu XG. Meeting the global food demand of the future by engineering crop photosynthesis and yield potential. *Cell.* 2015;161(1):56-66.

51. Ma Y, Pollock SV, Xiao Y, Cunnusamy K, Moroney JV. Identification of a Novel Gene, CIA6, Required for Normal Pyrenoid Formation in *Chlamydomonas reinhardtii*. *Plant Physiol*. 2011;156(2):884-896.

52. Machingura MC, Bajsa-Hirschel J, Laborde SM, Schwartzenburg JS, Mukherjee B, Mukherjee A, Pollock SV, Förster B, Price GD, Moroney JV. Identification and characterisation of a solute carrier, CIA8, involved in inorganic carbon acclimation in *Chlamydomonas reinhardtii. J Exp Bot.* 2017;68(14):3879-3890.

53. Mackinder LCM. The *Chlamydomonas* CO_2-concentrating mechanism and its potential for engineering photosynthesis in plants. *New Phytol.* 2018;217(1):54-61.

54. Mackinder LCM, Meyer MT, Mettler-Altmann T, Chen VK, Mitchell MC, Caspari O, Freeman Rosenzweig ES, Pallesen L, Reeves G, Itakura A, Roth R, Sommer F, Geimer S, Muhlhaus T, Schroda M, Goodenough U, Stitt M, Griffith H, Jonikas MC. A repeat protein links Rubisco to form the eukaryotic carbon-concentrating organelle. *Proc Nat Acad Sci USA*. 2016;113(21):5958-5963.

55. Mackinder LCM, Chen C, Leib RD, Patena W, Blum SR, Rodman M, Ramundo S, Adams CM, Jonikas MC. A Spatial Interactome Reveals the Protein Organization of the Algal CO_2 Concentrating Mechanism. *Cell*. 2017;171(1):133-147.

56. Mariscal V, Moulin P, Orsel M, Miller AJ, Fernández E, Galván A. Differential Regulation of the *Chlamydomonas* Nar1 Gene Family by Carbon and Nitrogen. *Protist*, 2006;157(4):421-433.

57. Messerli MA, Amarak-Zettler LA, Zettler E, Jung SK, Smith PJ, Sogin ML, Life at acidic pH imposes an increased energetic cost for a eukaryotic acidophile, *J Exp Biol.* 2005;208:2569-2579.

58. Milenkovic VM, Langmann T, Schreiber R, Kunzelmann K, Weber BH. Molecular evolution and functional divergence of the bestrophin protein family. *BMC Evol Biol.* 2008;8:72.

59. Miura K, Yamano T, Yoshioka S, Kohinata T, Inoue Y, Taniguchi F, Asamizu E, Nakamura Y, Tabata S, Yamato KT, Ohyama K, Fukuzawa H. *Plant Physiol.* 2004;135(3):1595-1607.

60. Mooij T, Vries G, Latsos C, Wijffels RH, Janssen M. Impact of light color on photobioreactor productivity, *Algal Research*, 2016;15:32-42.

61. Moroney JV, Husic HD, Tolbert NE. Effect of Carbonic Anhydrase Inhibitors on Inorganic Carbon Accumulation by *Chlamydomonas reinhardtii*. *Plant Physiol.* 1985;79(1):177-183.

62. Moroney JV, Tolbert NE, Sears BB. Complementation analysis of the inorganic carbon concentrating mechanism of *Chlamydomonas reinhardtii Molec. Gen. Genet.* 1986;204(2):199-203.

63. Morita E, Abe T, Tsuzuki M, Fujiwara S, Sato N, Hirata A, Sonoike K, Nozaki H. Presence of the CO_2-concentrating mechanism in some species of the pyrenoid-less free-living algal genus *Chloromonas* (Volvocales, Chlorophyta). *Planta.* 1998;204(3): 269-276.

64. Nugent T, Jones DT. Transmembrane protein topology prediction using support vector machines. BMC Bioinformatics, 2009;10:159.

65. Ouyang J, Shao X, Li J. Indole-3-glycerol phosphate, a branchpoint of indole-3-acetic acid biosynthesis from the tryptophan biosynthetic pathway in Arabidopsis thaliana. *Plant J.* 2000;24(3): 327-334.

66. Pedersen O, Colmer TD, Sand-Jensen K. Underwater photosynthesis of submerged plants - recent advances and methods. *Front Plant Sci*. 2013;4:140.

67. Perrine Z, Negi S, Sayre RT. Optimization of photosynthetic light energy utilization by microalgae, *Algal Research*, 2012;1(2):134-142.

68. Peterhansel C, Horst I, Niessen M, et al. Photorespiration. Arabidopsis Book. 2010;8:e0130.

69. Pollock SV, Prout DL, Godfrey AC, Lemaire SD, Moronet JV. The *Chlamydomonas reinhardtii* proteins Ccp1 and Ccp2 are required for long-term growth, but are not necessary for efficient photosynthesis, in a low-CO_2 environment. *Plant Mol Biol.* 2004;56(1): 125-132.

70. Polukhina I, Fristedt R, Dinc E, Cardol P, Croce R. Carbon Supply and Photoacclimation Cross Talk in the Green Alga *Chlamydomonas reinhardtii. Plant Physiol.* 2016;172(3):1494-1505.

71. Pribil M, Labs M, Leister D; Structure and dynamics of thylakoids in land plants, *J Exp Bot.* 2014;65(8):1955–1972.

72. Price GD, Pengelly JJ, Forster B, Du J, Whitney SM, von Caemmerer S, Badger MR, Howitt SM, Evans JR. The cyanobacterial CCM as a source of genes for improving photosynthetic CO_2 fixation in crop species. *J Exp Bot.* 2013;64(3):753-768.

73. Porra RJ, Thompson WA, Kriedemann PE. Determination of accurate extinction coefficients and simultaneous equations for assaying chlorophylls a and b extracted with four different solvents: verification of the concentration of chlorophyll standards by atomic absorption spectroscopy. *Biochimica et biophysica Acta*. 1989;975(3):384-394.

74. Qu Z, Hartzell HC. Bestrophin Cl^- channels are highly permeable to HCO_3^-. *Am J Physiol Cell Physiol*. 2008;294(6):C1371-7.

75. Qu Z, Chien LT, Cui Y, Hartzell HC. The Anion-Selective Pore of the Bestrophins, a Family of Chloride Channels Associated with Retinal Degeneration. *J Neurosci.* 2006;26(20):5411-5419.

76. Reams AB, Roth JR. Mechanisms of gene duplication and amplification. *Cold Spring Harb Perspect Biol*. 2015;7(2):a016592.

77. Sage RF, Khoshravesh R, Sage TL; From proto-Kranz to C4 Kranz: building the bridge to C4 photosynthesis, *J Exp Bot*. 2014;65(13):3341–3356.

78. Schottkowski M, Peters M, Zhan Y, Rifai O, Zhang Y, Zerges W. Biogenic membranes of the chloroplast. *Proc Nat Acad Sci USA*. 2012l;109(47):19286-19291.

79. Schwede T, Kopp J, Guex N, Peitsch MC. SWISS-MODEL: An automated protein homology-modeling server. *Nucleic acids research*, 2003;31(13), 3381-5.

80. Sinetova MA, Kupriyanova EV, Markelova AG, Allakhverdiev SI, Pronina NA. Identification and functional role of the carbonic anhydrase Cah3 in thylakoid membranes of pyrenoid of *Chlamydomonas reinhardtii. Biochim Biophys Acta.* 2012;1817(8):1248-1255.

81. Spalding MH, Spreitzer RJ, Ogren WL. Carbonic Anhydrase-Deficient Mutant of *Chlamydomonas reinhardii* Requires Elevated Carbon Dioxide Concentration for Photoautotrophic Growth. *Plant Physiol*. 1983;73(2):268-272.

82. Sperschneider J, Catanzariti AM, DeBoer K, Petre B, Gardiner DM, Singh KB, Dodds PN, Taylor JM. LOCALIZER: subcellular localization prediction of both plant and effector proteins in the plant cell. *Sci Rep*. 2017;7:44598.

83. Sültemeyer DF, Miller AG, Espie GS, Fock HP, Canvin DT. Active CO_2 Transport by the Green Alga *Chlamydomonas reinhardtii. Plant Physiol*. 1989;89(4):1213-1219.

84. Tachiki A, Fukuzawa H, Miyachi S. Characterization of Carbonic Anhydrase Isozyme CA2, Which Is the CAH2 Gene Product, in *Chlamydomonas reinhardtii, Bioscience, Biotechnology, and Biochemistry*. 1992; 56 (5): 794-798.

85. Tardif M, Atteia A, Specht M, Cogne G, Rolland N, Brugiere S, Hippler M, Ferro M, Bruley C, Peltier G, Vallon O, Cournac L. PredAlgo: a new subcellular localisation prediction tool dedicated to green algae. *Mol Biol Evol*. 2012;12:3625-39.

86. Tetteh NR. Chemical soil degradation as a result of contamination: A review. *J Soil Sci. Environ. Manage.* 2015;6(11):301-308.

87. Thever MD, Saier MH. Bioinformatic characterization of p-type ATPases encoded within the fully sequenced genomes of 26 eukaryotes. *J Membr Biol*. 2009;229(3):115-30.

88. Tsunenari T, Sun H, Williams J, Cahil H, Smallwood P, Yau KW, Nathans J. Structure-function analysis of the bestrophin family of anion channels. *J Biol Chem*. 2003;278(42):41114-25.

89. Uniacke J, Zerges W. Photosystem II Assembly and Repair Are Differentially Localized in *Chlamydomonas. The Plant Cell*. 2007;19(11):3640-3654.

90. Vaisey G, Miller AN, Long SB. Distinct regions that control ion selectivity and calcium-dependent activation in the bestrophin ion channel. *Proc Nat Acad Sci USA.* 2016;113(47):E7399-E7408.

91. Van Gunsteren WF, Berendsen HJC. Biomolecular Simulation: The GROMOS 96 Manual and User Guide. *VDF Hochschulverlag AG an der ETH Zürich, Zürich*, 1996,1-1042.

92. Van K, Spalding M. Periplasmic Carbonic Anhydrase Structural Gene (Cah1) Mutant in *Chlamydomonas reinhardtii. Plant Physiol.* 1999; 120(3): 757-764

93. Vance P, Spalding MH. Growth, photosynthesis, and gene expression in *Chlamydomonas* over a range of CO_2 concentrations and CO_2/O_2 ratios: CO_2 regulates multiple acclimation states. *Can J Bot*. 2005;83(7):796-809.

94. Villarejo A, Martinez F, del Pino Plumed M, Ramazanov Z. The induction of the CO_2 concentrating mechanism in a starch-less mutant of *Chlamydomonas reinhardtii. Physiologia Plantarum*, 1996;98(4): 798-802.

95. Villarejo A, Shutova T, Moskvin O, Forssén M, Klimov VV, Samuelsson G. A photosystem II-associated carbonic anhydrase regulates the efficiency of photosynthetic oxygen evolution. *The EMBO Journal*, 2002;21(8):1930-1938.

96. Von Caemmerer S, Quick PW, Furbank RT. The Development of C4 Rice: Current Progress and Future Challenges. *Science,* 2012;336(6089):1671-1672

97. Wang L, Yamano T, Takane S, et al. Chloroplast-mediated regulation of CO_2-concentrating mechanism by Ca^{2+}-binding protein CAS in the green alga *Chlamydomonas reinhardtii. Proc Nat Acad Sci USA.* 2016;113(44):12586-12591.

98. Wang YJ, Spalding MH. Acclimation to Very Low CO_2: Contribution of Limiting CO_2 Inducible Proteins, LCIB and LCIA, to Inorganic Carbon Uptake in *Chlamydomonas reinhardtii. Plant Physiol.* 2014;166(4):2040-2050.

99. Wang Y, Stessman DJ, Spalding MH. The CO_2 concentrating mechanism and photosynthetic carbon assimilation in limiting CO_2: how *Chlamydomonas* works against the gradient. *Plant J.* 2015;82:429-448.

100. Waterhouse A, Bertoni M, Bienert S, Studer G, Tauriello G, Gumienny R, Heer FT, de Beer TAP, Rempfer C, Bordoli L, Lepore R, Schwede T. SWISS-MODEL: homology modelling of protein structures and complexes. *Nucleic Acids Res*. 2018;46(W1):W296-W303.

101. Williams TG, Turpin DH. The Role of External Carbonic Anhydrase in Inorganic Carbon Acquisition by *Chlamydomonas reinhardii* at Alkaline pH. *Plant Physiol.* 1987;83(1):92-96.

102. Wittkopp TM, Saroussi S, Yang W, Johnson X, Kim RG, Heinnickel ML, Russel JJ, Phuthong W, Dent RM, Broeckling CD, Peers G, Lohr M, Wollman FA, Niyogi KN, Grossman AR. GreenCut protein CPLD49 of *Chlamydomonas reinhartii* associates with thylakoid membranes and is required for cytochrome b_6f complex accumulation. *Plant J.* 2018;94(6):1023-1037.

103. Wood WH, MacGregor-Chatwin C, Barnett SF, Mayneord GE, Huang X, Hobbs JK, Hunter CN, Johnson MP. Dynamic thylakoid stacking regulates the balance between linear and cyclic photosynthetic electron transfer; *Nature Plants,* 2018;4:116–127.

104. Wunder T, Cheng SH, Li HY, Mueller-Cajar O. The phase separation underlying the pyrenoid-based microalgal Rubisco supercharger. *Nat Commun.* 2018;9(1):5076.

105. Yamano T, Miura K, Fukuzawa H. Expression Analysis of Genes Associated with the Induction of the Carbon-Concentrating Mechanism in Chlamydomonas reinhardtii. *Plant Physiol.* 2008;147:(1) 340-354.

106. Yamano T, Sato E, Iguchi H, Fukuda Y, Fukuzawa H. Characterization of cooperative bicarbonate uptake into chloroplast stroma in the green alga *Chlamydomonas reinhardtii. Proc Natl Acad Sci USA*. 2015;112(23):7315-20.

107. Yamano T, Tsujikawa T, Hatano K, Ozawa SC, Takahashi Y, Fukuzawa H. Light and Low-CO_2-Dependent LCIB–LCIC Complex Localization in the Chloroplast Supports the Carbon-Concentrating Mechanism in *Chlamydomonas reinhardtii*, *Plant Cell Physiol*. 2010; 51(9):1453–1468.

108. Yang T, Liu Q, Kloss B, et al. Structure and selectivity in bestrophin ion channels. *Science*. 2014;346(6207):355-9.

109. Ynalvez RA, Xiao Y, Ward A, Cunnusamy K, Moroney J. Identificaion and characterisation of two closely related β-carbonic anhydrases from *Chlamydomonas reinhardtii. Physiologia Plantarum.* 2008;133:15-26.

110. Xiao Q, Hartzell HC, Yu K. Bestrophins and Retinopathies. *Pflugers Archiv*. 2010;460(2):559-569.

111. Xiao Q, Prussia A, Yu K, Cui YY, Hartzell HC. Regulation of bestrophin Cl channels by calcium: role of the C terminus. *J Gen Physiol*. 2008;132(6):681-92.